

SEMIALGEBRAIC CONDITIONS FOR IDENTIFYING TRIANGLES IN PHYLOGENETIC NETWORKS

BRYAN CURRIE, AVIVA K. ENGLANDER, JOSE A. ESPARZA-LOZANO, ELIZABETH GROSS,
MAX HILL, COLBY LONG, DEVON OLDS, KAWIKA O’CONNOR, UDANI RANASINGHE,
AND CHRISTIN SUM

ABSTRACT. An important consideration for a model-based method of phylogenetic network inference is the identifiability of the network parameter of the model. A recurring theme in previous works exploring this issue is that it is often difficult to identify the orientation of edges in a triangle of the network. In fact, it has been shown that for some models it is impossible to determine the orientation of triangle edges utilizing the standard algebraic technique of phylogenetic invariants. In this work, we consider one such model with a Jukes-Cantor site-substitution process and no coalescence. We give a complete semialgebraic description of three, 3-leaf Jukes-Cantor phylogenetic network models with embedded triangles. By describing these base cases, we resolve several questions about the identifiability of networks with embedded triangles. We show that for any pair of models, the intersection and set differences of the models are full-dimensional regions of the space of site-pattern probability distributions. Thus, despite being algebraically indistinguishable, these network models are not identical, nor are they identifiable (or generically identifiable). Our results also yield a straightforward biological interpretation—that the signal from a hybridization event may be immediately detectable but decays over time until it is impossible to identify the orientation of edges in the triangle of a network.

1. INTRODUCTION

A phylogenetic network model represents non-tree-like evolution along a directed acyclic graph. In such a model, network nodes of in-degree two correspond to reticulation events, such as hybridization or lateral gene transfer, where a certain proportion of the information at the node is assumed to have been inherited along each of the incoming edges. Recognizing that reticulation events are likely common in the evolutionary history of many species, there has been increasing interest in the theory of phylogenetic network models of DNA sequence evolution and their application to phylogenetic inference (Barley et al., 2022; Cui et al., 2013; Gambette et al., 2017; Hibbins and Hahn, 2022; Mallet et al., 2016; Pardi and Scornavacca, 2015; Rose et al., 2025; Solís-Lemus and Ané, 2016; van der Heijden et al., 2025; Zhang et al., 2018).

One important consideration for developing model-based methods of phylogenetic inference is the identifiability of the model parameters. In general, a model parameter is identifiable if it can be uniquely recovered from some output of the model. In the ideal case for phylogenetic inference, the observed data will perfectly fit a phylogenetic model and the corresponding model parameters are inferred. However, for this inference to be consistent, there must be a unique set of parameters corresponding to the data, that is, the parameters must be identifiable. As we consider the specific setting of networks, the same holds: to develop a consistent model-based method of network inference, the network parameter of the model must be identifiable. Several works have studied identifiability in phylogenetic

network models with and without a coalescent process (Allman et al., 2025, 2024, 2022; Baños, 2019; Englander et al., 2025; Gross and Long, 2018; Gross et al., 2021; Holtgreffe et al., 2025; Rhodes et al., 2025; Xu and Ané, 2023).

One recurring theme in these works is that while many network features are identifiable from data, it is often not possible to identify network *triangles* or to determine the orientation of edges in a triangle of the network. For example, the results of Gross and Long (2018) establish only the identifiability of *triangle-free* networks, and the standard methods of algebraic statistics employed therein are unable to distinguish networks such as those shown in Figure 1. Likewise, Barton et al. (2026); Englander et al. (2025); Gross et al. (2021) and Holtgreffe et al. (2025) also consider only triangle-free networks due to the inadequacy of algebraic methods for distinguishing triangles. It is thought that hybridization is negatively correlated with genetic distance between species (Mallet, 2005). Since reticulation is expected to be most common among closely related species, triangles are likely an important part of the evolutionary history of many sets of taxa, making the gap in the current results especially unfortunate. One notable exception to this trend are the results of Allman et al. (2024), who showed that under the network multispecies coalescent model, 3-cycles can sometimes be detected from gene tree quartet concordance factors.

The results of Englander et al. (2025); Gross and Long (2018) and Gross et al. (2021) apply to DNA sequence models without a coalescent process. Here, each choice of parameters produces a probability distribution on the possible DNA site-patterns that may be observed in the aligned DNA sequences of the species under consideration. The algebraic approach used to prove the identifiability of the network parameter is based on finding *phylogenetic invariants* for each network. These are polynomial relationships that are always satisfied by the site-pattern probability distributions coming from a model on the network. The key idea is to show that every pair of networks is *algebraically distinguishable*, that is, there is a polynomial invariant for each that is not an invariant for the other. Thus, given a site-pattern probability distribution from a network model, one can evaluate the invariants at the distribution to determine the network parameter that produced the data. This is a standard technique in algebraic statistics and phylogenetic invariants have been used to establish many identifiability results (Sullivant, 2023, Chapter 15, p.335-370). Often, the approach is to first find phylogenetic invariants for trees or networks with just a few taxa using computational tools, and then, to use combinatorial arguments and restrictions to subsets of taxa to show that trees or networks with an arbitrary number of leaves are distinguishable.

As noted above, despite the power of the algebraic approach, for certain models these methods are simply insufficient to establish the identifiability of networks with embedded triangles. For example, under the Jukes-Cantor model, there are no phylogenetic invariants for the three networks shown in Figure 1 and so they are not algebraically distinguishable.

For those familiar with considering phylogenetic models from an algebraic statistics perspective, the fact that there are no invariants for these networks means that each of the models is a full-dimensional subset of the probability simplex and its Zariski closure fills the entire space. However, although their Zariski closures are equal, the example below gives some intuition for why we may not expect the models themselves to be equal.

Example 1.1. Consider the site-pattern probability distribution generated by the Jukes-Cantor model on \mathcal{N}_1 , the rooted 3-leaf network from Figure 1. Figure 2 (left) shows this network with branch lengths given in expected number of mutations per site. The dotted

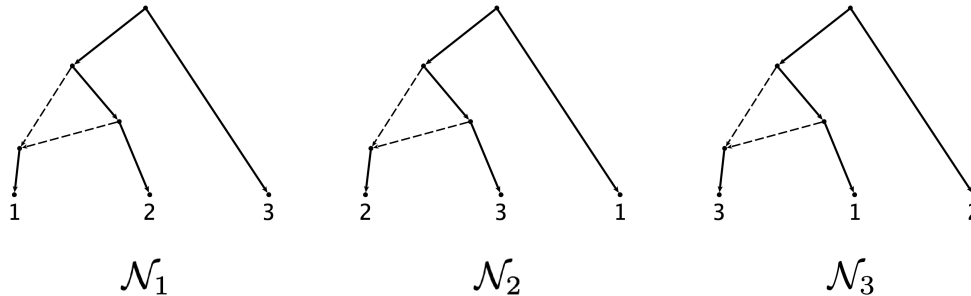


FIGURE 1. The three 3-leaf level-one triangle networks, each rooted on one of the non-hybrid leaf edges.

reticulation edges are length $\epsilon > 0$ and represent a near instantaneous hybridization event. For this example, we assume half of the genetic information is inherited along each edge.

If ℓ is sufficiently large, then the sites observed at leaves 2 and 3 are nearly independent. If it is also the case that s is very small, then the resulting site pattern probability distribution from the model represents essentially a coin flip as to whether the site observed at leaf 1 is identical to the site at leaf 2 or at leaf 3. It seems impossible for such a distribution to result from any choice of branch lengths and reticulation parameter for networks \mathcal{N}_2 or \mathcal{N}_3 . Indeed, by applying the results of Corollary 3.3, we can show that for fixed ℓ , when s is below a certain threshold the resulting site-pattern probability distribution does not belong to the models on networks \mathcal{N}_2 and \mathcal{N}_3 . The biological interpretation of this result is rather straightforward—it is generally possible to identify the precise nature of a hybridization event immediately after it occurs, but this signal decays until it eventually becomes impossible to determine the orientation of edges in the triangle of the network.

Figure 2 (right) shows this relationship explicitly for the limiting case as $\epsilon \rightarrow 0$. In the figure, points (s, ℓ) in the shaded region result in distributions that belong exclusively to the model on \mathcal{N}_1 . For a fixed ℓ , as s increases we eventually approach the threshold of identifiability beyond which it is impossible to determine the orientation of edges in the triangle. As $\ell \rightarrow \infty$, the boundary threshold for s approaches the asymptote $s = \ell - \frac{3}{4} \log(4)$, and as $\ell \rightarrow 0$, it approaches $\ell = (1 + \sqrt{5})s$. The second asymptote implies that when ℓ is small (the biologically relevant case), distinguishing the hybrid node requires s to be less than approximately $\ell/(1 + \sqrt{5}) \approx \ell/3.2$.

If the models are not equal, it is possible that there are polynomial *inequalities* that hold for each model that would allow us to distinguish them. Such inequalities have also been used to establish identifiability for phylogenetic models (Allman et al., 2024; Englander et al., 2025).

In this work, we consider the Jukes-Cantor model on the 3-leaf phylogenetic networks with embedded triangles shown in Figure 1. By finding polynomial inequalities for these base case models, we are able to resolve several questions about the identifiability of networks with embedded triangles. For example, our results show that in general these networks are not identifiable (or generically identifiable), however, we also show that none of the 3-leaf triangle network models are identical. That is, each network model contains site-pattern probability distributions that do not belong to the other two models.

The remainder of our paper proceeds as follows. In *Materials and Methods*, we describe the phylogenetic network models and their parameterizations in the Fourier coordinates. In

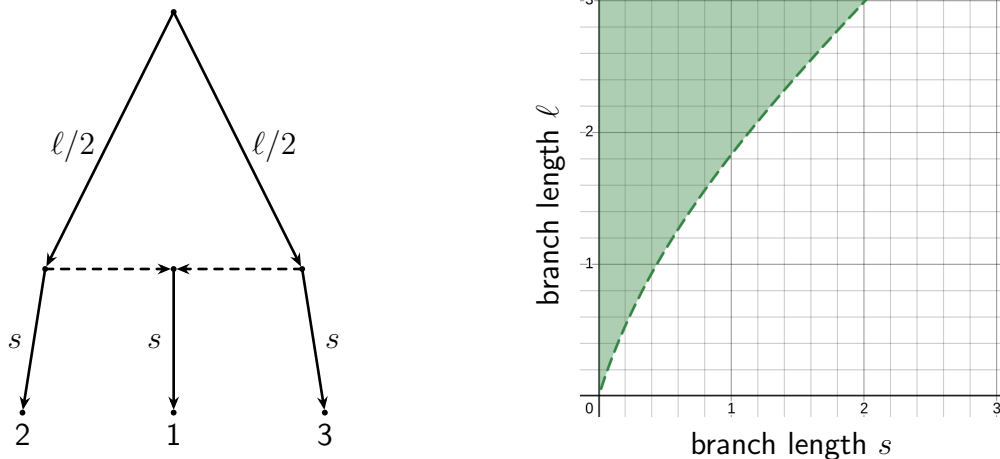


FIGURE 2. Left: The network \mathcal{N}_1 from Figure 1, with branch lengths given in expected number of mutations per site. Right: The shaded region represents the choices of branch lengths (in terms of s and ℓ) for which the resulting site-pattern probability distributions belong exclusively to the model on \mathcal{N}_1 .

Results, we first describe the identifiability of numerical parameters within a single model, and then give a complete semialgebraic description of the network model for \mathcal{M}_1 , the model on \mathcal{N}_1 . In the subsection *Model Intersections and Implications for Identifiability*, we apply the above results to explore the intersections of all three Jukes-Cantor 3-leaf triangle network models, including giving necessary and sufficient conditions in terms of the numerical parameters for the resulting site-pattern probability distribution to lie in the intersection of two or more models. We then further explore the size of model intersections. Finally, we present two applications to biological data and discuss the implications of these results for the identifiability and practical inference of phylogenetic networks.

2. MATERIALS AND METHODS

A distribution in a phylogenetic network model of DNA sequence evolution can be viewed as a mixture of tree distributions. Thus we begin this section by describing tree-based Markov models of DNA sequence evolution.

2.1. Phylogenetic Tree Models. Let \mathcal{T} be a rooted n -leaf binary phylogenetic tree with leaves labeled by the taxa in $[n] = \{1, \dots, n\}$ and root vertex ρ . To each vertex v of \mathcal{T} , we associate a random variable X_v with state space the set of four DNA bases $\{\mathbf{A}, \mathbf{G}, \mathbf{C}, \mathbf{T}\}$. The state of this random variable represents the nucleotide at the site being modeled in the DNA sequence of the taxon represented by the vertex v .

The *root distribution* of the model, $\boldsymbol{\pi}$, specifies the probability of observing each of the four DNA bases at the root of the tree. We associate to each edge of \mathcal{T} a 4×4 Markov transition matrix with rows and columns indexed by the four DNA bases. The entries of these matrices describe the rates of mutation along each edge, that is, for edge $e = uv$ of \mathcal{T} , $M_{ij}^e = P(X_v = j \mid X_u = i)$. We refer to the root distribution and the entries of the transition matrices as the *numerical parameters* of the model.

Given an assignment of states to the vertices of \mathcal{T} ,

$$\phi : V(\mathcal{T}) \rightarrow \{\mathbf{A}, \mathbf{G}, \mathbf{C}, \mathbf{T}\},$$

we can compute the probability of observing this particular assignment of states using the root distribution and the transition matrices as

$$p(\phi) = \pi_{\phi(\rho)} \prod_{e \in E(\mathcal{T})} M_{\phi(u), \phi(v)}^e.$$

To compute the probability of observing a particular *site-pattern* (X_1, \dots, X_n) in the aligned DNA sequences of the taxa at the leaves, we compute the joint distribution of the leaves by marginalizing over all possible assignments of states to the interior vertices of \mathcal{T} . More formally, if $\phi|_{\mathcal{L}}$ is the n -tuple of states that ϕ assigns to the leaves \mathcal{L} of \mathcal{T} , then the probability of observing the site-pattern $\omega = (i_1, i_2, \dots, i_n)$ is

$$(1) \quad p_\omega = \sum_{\phi: \phi|_{\mathcal{L}} = \omega} p(\phi) = \sum_{\phi: \phi|_{\mathcal{L}} = \omega} \pi_{\phi(\rho)} \prod_{e \in E(\mathcal{T})} M_{\phi(u), \phi(v)}^e.$$

In this work, we will assume that the transition matrices come from a continuous-time Jukes-Cantor model of DNA sequence evolution. Thus, the root distribution is uniform, and each transition matrix M^e has the form

$$(2) \quad M_{ij}^e = \begin{cases} \frac{1}{4} + \frac{3}{4}e^{-4t/3} & \text{if } i = j \\ \frac{1}{4} - \frac{1}{4}e^{-4t/3} & \text{if } i \neq j \end{cases},$$

where t is the branch length in expected number of mutations per site (Jukes et al., 1969); see also (Semple et al., 2003, Chapter 8, pp.194-197).

For a fixed tree \mathcal{T} , the phylogenetic model defines a map

$$(3) \quad \psi_{\mathcal{T}} : \Theta_{\mathcal{T}} \rightarrow \Delta^{4^n - 1}$$

from the numerical parameter space $\Theta_{\mathcal{T}}$ for the model to the set of site-pattern probability distributions. The image of this map, $\mathcal{M}_{\mathcal{T}} = \text{im}(\psi_{\mathcal{T}})$, is the *phylogenetic model associated to \mathcal{T}* .

2.2. Phylogenetic Network Models. To define a site-substitution model on an n -leaf rooted binary phylogenetic network \mathcal{N} , we first specify a root distribution and then associate a transition matrix to each edge of \mathcal{N} just as for a phylogenetic tree model. Let w_1, \dots, w_m be the *reticulation vertices* of \mathcal{N} , the nodes of in-degree two, and let e_i^0 and e_i^1 be the edges directed into w_i .

To obtain a tree from the network, for each $i \in [m]$, we independently delete e_i^1 with probability $\delta_i \in (0, 1)$, and otherwise, we delete e_i^0 . Intuitively, the parameter δ_i corresponds to the probability that the particular site being modeled was inherited along edge e_i^0 . After deleting the m edges, the result is a rooted n -leaf phylogenetic tree. Each of these trees, along with its transition matrices inherited from \mathcal{N} , gives rise to a distribution in a phylogenetic tree model, and we can take a convex combination of these distributions to get a site-pattern

probability distribution from the network. For the networks we consider in this paper, there is only a single reticulation node, and so for each network we obtain a map

$$\begin{aligned} \psi_{\mathcal{N}} : \Theta_{\mathcal{N}} \times (0, 1) &\rightarrow \Delta^{4^n-1}, \\ (\theta, \delta) &\mapsto \delta\psi_{\mathcal{T}_1}(\theta) + (1 - \delta)\psi_{\mathcal{T}_2}(\theta). \end{aligned}$$

In the expression above, $\Theta_{\mathcal{N}} \times (0, 1)$ represents the numerical parameter space of the model, which includes the root distribution, transition matrices, and the single reticulation edge parameter δ chosen between 0 and 1. The trees \mathcal{T}_1 and \mathcal{T}_2 are the embedded trees of the network obtained by independently deleting e_1^1 and e_1^0 respectively. Just as for a tree, we define the image of this map, $\mathcal{M}_{\mathcal{N}} = \text{im}(\psi_{\mathcal{N}})$, to be the *phylogenetic model associated to the network* \mathcal{N} . Note that as in (Englander et al., 2025) we do not allow δ to be either 0 or 1. Thus, the models of the embedded trees are not contained in the network model.

Though these models are naturally defined in terms of rooted networks, because the Jukes-Cantor model is time-reversible, the location of the root in the network is unidentifiable (Gross et al., 2021). Thus, we can determine the parameterization of the phylogenetic model associated to the network \mathcal{N} from the semi-directed network obtained from \mathcal{N} by suppressing the root vertex and undirecting all edges other than the reticulation edges. For example, the semi-directed versions of $\mathcal{N}_1, \mathcal{N}_2$, and \mathcal{N}_3 from Figure 1 are depicted in Figure 3. For these three networks, we denote the corresponding phylogenetic models by $\mathcal{M}_1, \mathcal{M}_2$, and \mathcal{M}_3 .

2.3. The Fourier Coordinates. To compute the joint distribution at the leaves of a tree in a phylogenetic model, we sum over all possible states of the internal vertices. For one of the 3-leaf triangle networks of Figure 1, after we delete a reticulation edge, the resulting tree has five edges, each with their own transition matrix, and three internal vertices. Thus, following Eq. (1), each coordinate of the map $\psi_{\mathcal{T}_i}$ is parameterized by a degree 5 polynomial with $4^3 = 64$ terms. As a convex sum of $\psi_{\mathcal{T}_1}$ and $\psi_{\mathcal{T}_2}$, the parameterization of the network is even more complex, making it difficult to perform algebraic computations or to obtain a semialgebraic description of the model. Thus, we will apply a linear change of coordinates called the discrete Fourier transform that is defined for the Jukes-Cantor model as well as a broader class of models known as *group-based models* (Evans and Speed, 1993). In these new coordinates, the phylogenetic tree models are parameterized by monomials, which makes computations much more tractable. The Jukes-Cantor model is a group-based model, and we give a brief outline here of how to obtain the parameterization of the network in these new coordinates. It is not necessary to state all of the definitions surrounding group-based models and the discrete Fourier transform in order to describe the parameterization, so we do not delve into the details here and refer the interested reader instead to Sturmfels and Sullivant (2005) and (Sullivant, 2023, Chapter 15, pp. 335-370).

For what follows, we will assume that the tree \mathcal{T} is *unrooted*. We identify the state space $\{\mathbf{A}, \mathbf{G}, \mathbf{C}, \mathbf{T}\}$ with the Klein four-group $\mathbb{Z}_2 \times \mathbb{Z}_2$ as follows: $\mathbf{A} = (0, 0)$, $\mathbf{G} = (1, 0)$, $\mathbf{C} = (0, 1)$, $\mathbf{T} = (1, 1)$. We associate to each edge $e_i \in E(\mathcal{T})$ the four eigenvalues of its transition matrix M^{e_i} , which we refer to as the *Fourier parameters*, denoted $a_{\mathbf{A}}^i, a_{\mathbf{G}}^i, a_{\mathbf{C}}^i$ and $a_{\mathbf{T}}^i$. The largest of these, $a_{\mathbf{A}}^i$, is always 1 since M^{e_i} is a stochastic matrix. Due to symmetries of the Jukes-Cantor model, the remaining three Fourier parameters satisfy $a_{\mathbf{C}}^i = a_{\mathbf{G}}^i = a_{\mathbf{T}}^i = e^{-4t_i/3}$, where t_i is the branch length of e_i in expected number of mutations per site. Hence there is really only a single Fourier parameter a_i for each edge e_i , namely,

$$(4) \quad a_i = e^{-4t_i/3}.$$

For this paper, we will assume that each branch length t_i is finite and positive. Notice that since $t_i > 0$, the corresponding Fourier parameter a_i lies in the interval $(0, 1)$. The parameter a_i can be regarded as a measure of the nucleotide transmission fidelity along its edge, a quantity which decreases to 0 as the branch length t_i increases.

The Fourier transform extends to a transformation of the coordinate space, from probability coordinates to what we will call q -coordinates. The *Fourier parameterization*, which gives us the value of the q -coordinate q_ω for the site-pattern $\omega = (g_1, g_2, \dots, g_n) \in \{\mathbf{A}, \mathbf{G}, \mathbf{C}, \mathbf{T}\}^n$, is defined as

$$(5) \quad q_\omega = \begin{cases} \prod_{\substack{e_i \in E(\mathcal{T}) \\ e_i \text{ induces the split } A|B}} a_i^{\sum_{j \in A} g_j} & \text{if } \sum_{j=1}^n g_j = 0, \\ 0 & \text{otherwise} \end{cases}$$

where addition is in the group $\mathbb{Z}_2 \times \mathbb{Z}_2$.

These q -coordinates are not interpretable as probabilities; however, there is an inverse Fourier transform that allows us to convert back and forth between the q -coordinates and the probability coordinates (see Appendix B). Thus, a semialgebraic description of a model in terms of q -coordinates can be transformed to obtain a semialgebraic description of the model in probability coordinates (and vice versa). For the rest of this paper we will work in the Fourier coordinates, and for simplicity, we will use $\mathcal{M}_1, \mathcal{M}_2$, and \mathcal{M}_3 for the transformed models in the space of q -coordinates.

2.4. Parameterization of the 3-Leaf Jukes-Cantor Networks. In this section, we give the parameterization of the model \mathcal{M}_1 in Fourier coordinates using the semi-directed version of \mathcal{N}_1 with edges labeled as in Figure 3. From this parameterization, one can easily obtain parameterizations of \mathcal{M}_2 and \mathcal{M}_3 by permuting coordinates, as described below.

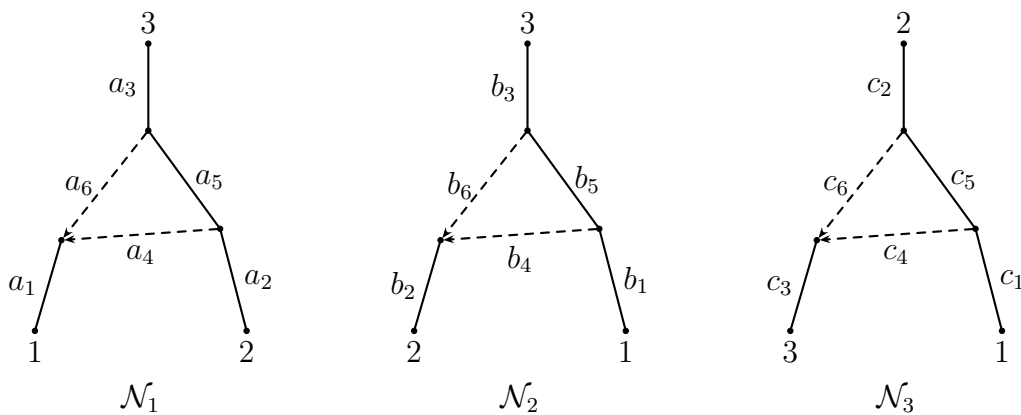


FIGURE 3. The three semi-directed networks corresponding to models $\mathcal{M}_1, \mathcal{M}_2$, and \mathcal{M}_3 , with associated Fourier edge parameters.

We begin by noting that because the Fourier transform gives a linear change of coordinates, for the network model, each q_ω is parameterized by a convex combination of the parameterizations for the displayed trees in Fourier coordinates. For example, if we delete the edge labeled a_6 with probability δ and the a_4 edge with probability $(1 - \delta)$ in the Jukes-Cantor model on the network \mathcal{N}_1 shown in Figure 3, then q_{CGT} , q_{GGA} , and q_{AAA} are parameterized as

follows:

$$\begin{aligned} q_{CGT} &= \delta a_C^1 a_G^2 a_T^3 a_C^4 a_T^5 + (1 - \delta) a_C^1 a_G^2 a_T^3 a_G^5 a_C^6 \\ q_{GGA} &= \delta a_G^1 a_G^2 a_A^3 a_G^4 a_A^5 + (1 - \delta) a_G^1 a_G^2 a_A^3 a_G^5 a_G^6 \\ q_{AAA} &= \delta a_A^1 a_A^2 a_A^3 a_A^4 a_A^5 + (1 - \delta) a_A^1 a_A^2 a_A^3 a_A^5 a_A^6. \end{aligned}$$

From Equation (5), we see that many coordinates for a group-based model on a tree are trivial after transformation, and the same coordinates will be trivial for the network model. Thus, for the 3-leaf network model, there are only 16 non-trivial coordinates to consider. We can also simplify the parameterization of many of these non-trivial coordinates. Since $a_A^i = 1$ for all $i \in [6]$, it is not necessary to include the a_A^i parameters (and hence, no need to consider the coordinate q_{AAA} which is equal to 1 for any choice of parameters for the model). Moreover, since $a_C^i = a_G^i = a_T^i$, several of the Fourier coordinates are always identical; for example, $q_{CCA} = q_{GGA} = q_{TTA}$.

After making these simplifications, there are only four non-trivial equivalence classes of Jukes-Cantor q -coordinates. We choose one representative from each of these equivalence classes, q_{ACC} , q_{CAC} , q_{CCA} , and q_{CGT} , to form the set of *simplified Jukes-Cantor q -coordinates*. For \mathcal{N}_1 , the simplified Jukes-Cantor q -coordinates are parameterized as follows:

$$(6) \quad \begin{aligned} q_{ACC} &= a_2 a_3 a_5 \\ q_{CAC} &= \delta a_1 a_3 a_4 a_5 + (1 - \delta) a_1 a_3 a_6 \\ q_{CCA} &= \delta a_1 a_2 a_4 + (1 - \delta) a_1 a_2 a_5 a_6 \\ q_{CGT} &= \delta a_1 a_2 a_3 a_4 a_5 + (1 - \delta) a_1 a_2 a_3 a_5 a_6 \end{aligned}$$

where $a_1, \dots, a_6 \in (0, 1)$ and $\delta \in (0, 1)$.

Working in the simplified Jukes-Cantor q -coordinates, the parameter space becomes

$$\Theta_{\mathcal{N}_1} = \{(a_1, \dots, a_6) : 0 < a_1, \dots, a_6 < 1\},$$

the parameterization map becomes

$$\begin{aligned} \psi_{\mathcal{N}_1} : \mathbb{R}^7 &\rightarrow \mathbb{R}^4 \\ (a_1, a_2, a_3, a_4, a_5, a_6, \delta) &\mapsto (q_{ACC}, q_{CAC}, q_{CCA}, q_{CGT}), \end{aligned}$$

and the model becomes

$$\mathcal{M}_1 = \{\psi_{\mathcal{N}_1}(\theta) : \theta \in \Theta_{\mathcal{N}_1} \times (0, 1)\} \subseteq \mathbb{R}^4.$$

3. RESULTS

In this section, we begin by describing the non-identifiability of the numerical parameters for a single 3-leaf triangle network model.

3.1. Identifiability of Numerical Parameters. The numerical parameters of the 3-leaf network model are not identifiable. Indeed, only the products $\delta a_1 a_4$ and $(1 - \delta) a_1 a_6$ are recoverable at best. Thus, for any choice of $a_1, a_2, a_3, a_4, a_5, a_6, \delta \in (0, 1)$, we can describe a two-dimensional region R of parameter space for which the map $\psi_{\mathcal{N}_1}$ sends every point of R to the same point in the model. For example, for any $\theta = (a_1, \dots, a_6, \delta) \in \Theta_{\mathcal{N}_1} \times (0, 1)$,

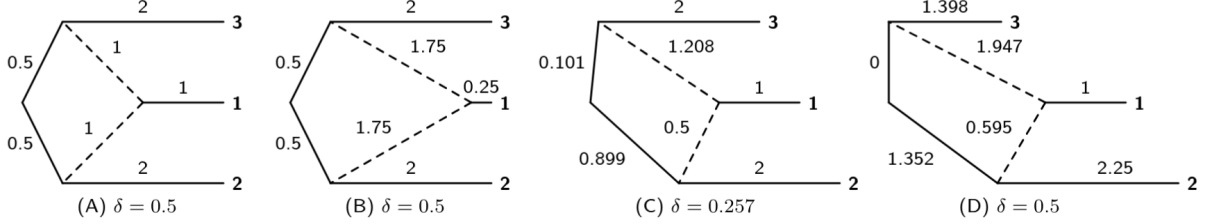


FIGURE 4. Networks (A)-(D) show four different choices of branch lengths for \mathcal{N}_1 that all give rise to the same site-pattern probability distribution. The networks are rooted along edge e_5 for display, but as noted above, the location of the root is not identifiable. Branch lengths, measured in expected number of mutations per site, are displayed in the figure as horizontal distances.

we can construct a new set of parameters $\theta' \in \Theta_{\mathcal{N}_1} \times (0, 1)$ such that $\psi_{\mathcal{N}_1}(\theta) = \psi_{\mathcal{N}_1}(\theta')$ by taking

$$(7) \quad \theta' = \left(\beta_1 a_1, a_2, a_3, \frac{a_4}{\beta_1 \beta_2}, a_5, \frac{a_6(1-\delta)}{\beta_1(1-\beta_2\delta)}, \beta_2 \delta \right)$$

for any choice of β_1, β_2 in appropriate open intervals of the positive real numbers containing 1.

The networks shown in Figure 4 illustrate this non-identifiability of the numerical parameters. First, we assign branch lengths to the network \mathcal{N}_1 in Figure 3 to obtain network (A). For network (A), the edges e_1, e_4, e_5 and e_6 are all length 1, the edges e_2 and e_3 are length 2, and $\delta = \frac{1}{2}$. Recall that the Fourier parameter corresponding to the edge e_i of length t_i is $a_i = e^{-4t_i/3}$. Thus, the Fourier parameters for network (A) are $a_1 = a_4 = a_5 = a_6 = e^{-4/3}$ and $a_2 = a_3 = e^{-8/3}$. Networks (B) and (C) are obtained by scaling the parameters according to Eq. (7) and then converting the Fourier parameters to branch lengths. In particular, network (B) is obtained by setting $\beta_1 = e$ and $\beta_2 = 1$, and network (C) by setting $\beta_1 = 1$ and $\beta_2 = e^{-2/3}$.

To account for the non-identifiability of a_1, a_4, a_6 , and δ , in our proof of Theorem 3.1 we will reparameterize the model by making the substitutions $a_4^* = \delta a_1 a_4$ and $a_6^* = (1-\delta)a_1 a_6$ (see Appendix A for details). The new parameters a_4^* and a_6^* must satisfy the additional restriction that $a_4^* + a_6^* < 1$ but are otherwise free. Yet, even after introducing a_4^* and a_6^* , the map is still not one-to-one. For a generic point $\mathbf{q} \in \mathcal{M}_1$, the fiber is a one-dimensional region of \mathbb{R}^5 , which is described in detail in Lemma A.3. Thus, since there is an additional degree-of-freedom, if we perturb one of the Fourier parameters, we can adjust the others so that the corresponding point in the model remains unchanged. Network (D) in Figure 4 is one such network, where beginning with network (A), we increase the length of edge e_2 by $1/4$, and adjust all other parameters accordingly.

3.2. A Semialgebraic Description of the Jukes-Cantor 3-Leaf Triangle Network Models. We now give a complete semialgebraic description of \mathcal{M}_1 in the space of simplified Jukes-Cantor q -coordinates. Combined with the results above, this will allow us to characterize the intersections of $\mathcal{M}_1, \mathcal{M}_2$, and \mathcal{M}_3 to gain insight into the question of network identifiability.

Theorem 3.1 (Semialgebraic description of \mathcal{M}_1). *Let $\mathbf{q} = (q_{\text{ACC}}, q_{\text{CAC}}, q_{\text{CCA}}, q_{\text{CGT}})$. Then $\mathbf{q} \in \mathcal{M}_1$ if and only if the following inequalities hold:*

$$(8) \quad 0 < q_{\text{ACC}}, q_{\text{CAC}}, q_{\text{CCA}}, q_{\text{CGT}} < 1$$

$$(9) \quad q_{\text{ACC}} - q_{\text{CGT}} > 0$$

$$(10) \quad q_{\text{CGT}} - q_{\text{ACC}}q_{\text{CAC}} > 0$$

$$(11) \quad q_{\text{ACC}}q_{\text{CAC}}q_{\text{CCA}} - q_{\text{CGT}}^2 > 0$$

$$(12) \quad q_{\text{CGT}} + q_{\text{ACC}}(q_{\text{CGT}} - q_{\text{CAC}} - q_{\text{CCA}}) > 0.$$

Moreover, if $\mathbf{q} \in \mathcal{M}_1$ then the following inequalities also hold:

$$(13) \quad q_{\text{CAC}} - q_{\text{CGT}} > 0$$

$$(14) \quad q_{\text{CCA}} - q_{\text{CGT}} > 0$$

$$(15) \quad q_{\text{CGT}} - q_{\text{ACC}}q_{\text{CCA}} > 0.$$

We defer the proof of Theorem 3.1 to Appendix A. Note that by symmetries, we can easily obtain similar descriptions of \mathcal{M}_2 and \mathcal{M}_3 by permuting the indices appropriately, i.e., by swapping the first and second index or by swapping the first and third. Note that inequalities (8), (9), (11), (13), and (14) appear in the description for all three models, and thus, are not informative about the location of the hybrid node. Inequalities (10) and (15) each appear in two of the three model descriptions and thus are only partially informative.

The linear inequalities (9), (13), and (14) are readily interpretable in terms of the two displayed trees. For example, if we restrict to the parameterization for the tree containing edge e_4 (this can be done by setting $\delta = 1$), we see that inequality (9) says that leaf node 1 in Figure 3 does not lie on the path between leaves 2 and 3 in the displayed tree containing e_4 . To see why this is the case, observe that setting $\delta = 1$ in Eq. (6) yields

$$(16) \quad q_{\text{ACC}} - q_{\text{CGT}} = a_2a_3a_5(1 - a_1a_4) \geq 0.$$

If the edges e_2, e_3 , and e_5 are finite then this is 0 if and only if $a_1 = a_4 = 1$ or equivalently, $t_1 = t_4 = 0$. A similar situation holds when considering the displayed tree containing e_6 . Since the network distribution is a convex sum of the tree distributions, the linear inequality Eq. (16) holds strictly for the network as well.

Inequality (11) also has an interesting interpretation that was first noted by Englander et al. (2025). Substituting a site-pattern distribution from any of the three 3-leaf networks into this polynomial will yield a positive value. But, the polynomial $q_{\text{ACC}}q_{\text{CAC}}q_{\text{CCA}} - q_{\text{CGT}}^2$ is an algebraic invariant for the 3-leaf claw tree under the Jukes-Cantor model. Thus, this invariant distinguishes the 3-leaf tree model from the 3-leaf network models, and the invariant residual may provide evidence of hybridization.

The other inequalities in Theorem 3.1 are less illuminating. When converted to the probability coordinates, inequalities (10) and (15) are irreducible degree 2 polynomials with 20 terms and inequality (12) is an irreducible degree 2 polynomial with 18 terms, and none of these have a readily apparent biological interpretation.

3.3. Model Intersections and Implications for Identifiability. In this section, we prove our main result (Theorem 3.5) regarding the identifiability of 3-cycles in a phylogenetic network model. In practical terms, Theorem 3.5 implies that if edge parameters are chosen randomly, then with positive probability, determining which of the three leaves is descended from the hybrid node is impossible even with infinite data.

First, we show the sets $\mathcal{M}_1 \setminus \mathcal{M}_2$ and $\mathcal{M}_1 \cap \mathcal{M}_2$ are separated by a single algebraic curve; namely, $q_{\text{CGT}} + q_{\text{CAC}}(q_{\text{CGT}} - q_{\text{ACC}} - q_{\text{CCA}}) = 0$.

Theorem 3.2. *Let $\mathbf{q} = (q_{\text{ACC}}, q_{\text{CAC}}, q_{\text{CCA}}, q_{\text{CGT}}) \in \mathcal{M}_1$. Then $\mathbf{q} \in \mathcal{M}_2$ if and only if*

$$(17) \quad q_{\text{CGT}} + q_{\text{CAC}}(q_{\text{CGT}} - q_{\text{ACC}} - q_{\text{CCA}}) > 0.$$

Similarly, $\mathbf{q} \in \mathcal{M}_3$ if and only if

$$(18) \quad q_{\text{CGT}} + q_{\text{CCA}}(q_{\text{CGT}} - q_{\text{ACC}} - q_{\text{CAC}}) > 0.$$

Proof. We prove only the case for \mathcal{M}_2 as the case for \mathcal{M}_3 is similar. As noted in the discussion following Theorem 3.1, by permuting indices of the Jukes-Cantor q -coordinates, we can easily derive defining sets of inequalities for the other two network models. In particular, by transposing the first two indices in the inequalities (8) through (12), and using the linear invariant $q_{\text{CGT}} - q_{\text{GCT}} = 0$ to write q_{GCT} as q_{CGT} , we find that the set \mathcal{M}_2 is defined by the inequality (17) together with the inequalities

$$(19) \quad \begin{aligned} 0 &< q_{\text{ACC}}, q_{\text{CAC}}, q_{\text{CCA}}, q_{\text{CGT}} < 1 \\ q_{\text{CAC}} - q_{\text{CGT}} &> 0 \\ q_{\text{CGT}} - q_{\text{CAC}}q_{\text{ACC}} &> 0 \\ q_{\text{ACC}}q_{\text{CAC}}q_{\text{CCA}} - q_{\text{CGT}}^2 &> 0. \end{aligned}$$

Suppose $\mathbf{q} \in \mathcal{M}_1$. It is easy to see that all of the inequalities in (19) are implied by inequalities in the statement of Theorem 3.1, since $\mathbf{q} \in \mathcal{M}_1$. Hence, $\mathbf{q} \in \mathcal{M}_2$ if and only if inequality (17) holds. \square

Theorem 3.2 establishes a criterion for determining whether a point $\mathbf{q} \in \mathcal{M}_1$ is in $\mathcal{M}_1 \setminus \mathcal{M}_2$ or $\mathcal{M}_1 \cap \mathcal{M}_2$. The next corollary, which will be useful for interpretation, expresses this inequality in terms of the numerical parameters a_1, \dots, a_6 , and δ , and follows immediately by substituting the parameterization of \mathcal{M}_1 into the inequalities (17) and (18).

Corollary 3.3 (Distinguishability criteria). *Let $\mathbf{q} \in \mathcal{M}_1$, and let $\theta = (a_1, a_2, a_3, a_4, a_5, a_6, \delta) \in \Theta_{\mathcal{N}_1} \times (0, 1)$ be a choice of numerical parameters such that $\psi_{\mathcal{N}_1}(\theta) = \mathbf{q}$. Then $\mathbf{q} \notin \mathcal{M}_2$ if and only if*

$$(20) \quad a_1 \geq \frac{a_5}{\delta a_4 a_5 + a_6(1 - \delta)} \cdot \frac{\delta a_4(1 - a_3 a_5) + a_6(1 - \delta)(1 - a_3)}{\delta a_4(1 - a_3 a_5) + a_5 a_6(1 - \delta)(1 - a_3)}.$$

Similarly, $\mathbf{q} \notin \mathcal{M}_3$ if and only if

$$(21) \quad a_1 \geq \frac{a_5}{\delta a_4 + a_5 a_6(1 - \delta)} \cdot \frac{a_6(1 - \delta)(1 - a_2 a_5) + \delta a_4(1 - a_2)}{a_6(1 - \delta)(1 - a_2 a_5) + \delta a_4 a_5(1 - a_2)}.$$

The network parameter of these models is *generically identifiable* if the set of parameters that maps into the intersection of two models is measure zero within the parameter space. Theorem 3.5 states that this is not the case. To prove this, we will utilize the following lemma, in which we use the notation $\overline{\mathcal{M}_2}$ to denote the Euclidean closure of \mathcal{M}_2 .

Lemma 3.4. *Both $\mathcal{M}_1 \cap \mathcal{M}_2$ and $\mathcal{M}_1 \setminus \overline{\mathcal{M}_2}$ are nonempty open subsets of \mathbb{R}^4 .*

Proof. We begin by showing that $\mathcal{M}_1 \cap \mathcal{M}_2$ and $\mathcal{M}_1 \setminus \overline{\mathcal{M}_2}$ are open sets. By Theorem 3.1, \mathcal{M}_1 is the intersection of a finite number of open sets; namely, the sets corresponding to the strict inequalities in (8)-(12). Therefore \mathcal{M}_1 is open. Similarly, Theorem 3.2 implies that

$\mathcal{M}_1 \cap \mathcal{M}_2$ is open since it is the intersection of two open sets. Moreover, since \mathcal{M}_1 is open and $\overline{\mathcal{M}_2}$ is closed, $\mathcal{M}_1 \setminus \overline{\mathcal{M}_2}$ is open as well.

It remains to show that $\mathcal{M}_1 \cap \mathcal{M}_2$ and $\mathcal{M}_1 \setminus \overline{\mathcal{M}_2}$ are nonempty. To show that $\mathcal{M}_1 \cap \mathcal{M}_2 \neq \emptyset$, observe that for any choice of $a_1, a_2, a_3, a_4, a_6, \delta \in (0, 1)$, as $a_5 \rightarrow 1$, the right-hand side of inequality (20) tends to

$$\frac{1}{\delta a_4 + (1 - \delta)a_6} > 1.$$

Therefore we may choose a_5 sufficiently close to 1 so that the right-hand side of inequality (20) is larger than a_1 , in which case Corollary 3.3 implies $\psi_{\mathcal{N}_1}(a_1, a_2, a_3, a_4, a_5, a_6, \delta) \in \mathcal{M}_1 \cap \mathcal{M}_2$, and hence $\mathcal{M}_1 \cap \mathcal{M}_2 \neq \emptyset$. Similarly, to show that $\mathcal{M}_1 \setminus \overline{\mathcal{M}_2} \neq \emptyset$, observe that we may choose a_5 sufficiently close to zero so that the right-hand side of (20) is smaller than a_1 , in which case $\mathbf{q} = \psi_{\mathcal{N}_1}(a_1, a_2, a_3, a_4, a_5, a_6, \delta) \in \mathcal{M}_1 \setminus \overline{\mathcal{M}_2}$. \square

Lemma 3.4 can be understood as saying that $\mathcal{M}_1 \cap \mathcal{M}_2$ and $\mathcal{M}_1 \setminus \overline{\mathcal{M}_2}$ are both full-dimensional subsets of \mathbb{R}^4 . The proof of Theorem 3.5 now follows by a simple topological argument. In particular, since $\mathcal{M}_1 \cap \mathcal{M}_2$ is open by Lemma 3.4, it follows by continuity of $\psi_{\mathcal{N}_1}$ that $\psi_{\mathcal{N}_1}^{-1}(\mathcal{M}_1 \cap \mathcal{M}_2)$ is an open subset of the parameter space $\Theta_{\mathcal{N}_1} \times (0, 1) \subseteq \mathbb{R}^7$. Therefore, since $\psi_{\mathcal{N}_1}^{-1}(\mathcal{M}_1 \cap \mathcal{M}_2)$ is open, it is also both full-dimensional and of positive measure.

Theorem 3.5. *The semi-directed topology of a 3-leaf Jukes-Cantor triangle network model is **not** generically identifiable from the site pattern distribution.*

Although we have now shown that the network parameter is not generically identifiable, the story does not end here. Since $\mathcal{M}_1 \setminus \overline{\mathcal{M}_2}$ is open, it follows that $\psi_{\mathcal{N}_1}^{-1}(\mathcal{M}_1 \setminus \overline{\mathcal{M}_2})$ is open, and hence $\psi_{\mathcal{N}_1}^{-1}(\mathcal{M}_1 \setminus \overline{\mathcal{M}_2})$ contains an open set. Thus, there exists a full dimensional subset of parameter space on which it is theoretically possible to determine which of the three leaves is descendant from the hybrid node.

3.4. The Volume of Model Intersections. In this section, we take a closer look at the models and their intersections to better understand the practical implications of these results for phylogenetic inference. To estimate the relative volumes of the three models and their intersections, we sampled $n = 10^9$ points uniformly at random from the probability simplex Δ_4 using the Dirichlet(1, 1, 1, 1, 1) distribution and recorded the proportion of points whose Fourier transform satisfied the model inequalities. These results are summarized in Figure 5. The code for this and all subsequent simulations in this section are available in the file `model-size-simulations.jl` in the Supplementary Materials.

Observation 1 (Model overlap in the simplex). The three models $\mathcal{M}_1, \mathcal{M}_2$ and \mathcal{M}_3 correspond to small regions of the simplex which overlap substantially. Only about 3.7% of simplex points correspond to distributions in any of the three models, with each model accounting for only about 1.76% of simplex points. Moreover, of the simplex points which belong to a given model \mathcal{M}_i , almost half (47.9%) coincide with at least one of the other two models.

Since the Fourier transformation scales 4-dimensional volume in the simplex uniformly by a constant factor (see Appendix B), we can estimate the model volumes explicitly. The 4-dimensional volume of the space of simplified Jukes-Cantor coordinates is approximately 0.26337; within this space, each of the models $\mathcal{M}_1, \mathcal{M}_2$, and \mathcal{M}_3 has absolute volume approximately 0.00464, the volume of the intersection of any two models is approximately 0.00184,

and the volume of the intersection of all three is approximately 0.00147. See Remark 1 in Appendix B for details.

While these figures give some perspective on the geometry of the models and their intersections in the q -coordinates, the issue of identifiability is perhaps better illuminated by considering which *parameter* choices for a model give a site-pattern probability distribution that belongs to one or both of the other models. To investigate this, we sampled $n = 10^8$ numerical parameter vectors $(a_1, \dots, a_6, \delta)$ for \mathcal{N}_1 uniformly at random from $\Theta_{\mathcal{N}_1} \times (0, 1)$.

Observation 2 (Model overlap in the parameter space). We find that when parameters are sampled uniformly at random, about 94.3% of parameter choices yield a point in the intersection of two or more models, in which case the hybrid is not distinguishable. In particular, about 91.4% of parameter choices lie in $\psi_{\mathcal{N}_1}^{-1}(\mathcal{M}_1 \cap \mathcal{M}_2 \cap \mathcal{M}_3)$, about 92.8% lie in each of $\psi_{\mathcal{N}_1}^{-1}(\mathcal{M}_1 \cap \mathcal{M}_2)$ and $\psi_{\mathcal{N}_1}^{-1}(\mathcal{M}_1 \cap \mathcal{M}_3)$, and only 5.7% lie in $\psi_{\mathcal{N}_1}^{-1}(\mathcal{M}_1 \setminus (\mathcal{M}_2 \cup \mathcal{M}_3))$.

One limitation in interpreting these results is that the uniform sampling regime, while of interest geometrically, places excessive weight on very long branches which are not biologically realistic. To address this, we simulated networks with shorter, bounded branch lengths. For each $\delta \in \{.01, .02, \dots, .99\}$ and each $m \in \{.1, .25, .5, 1\}$, we sampled $n = 10^7$ sets of branch lengths $t_1, \dots, t_6 \stackrel{iid}{\sim} \text{unif}(0, m)$ for \mathcal{N}_1 .

The results of this simulation (shown in Fig. 6) indicate that the conditions needed for hybrid distinguishability are rarely satisfied for the sorts of branch lengths typically seen in phylogenetic inference. The proportion of hybrid distinguishable networks was always less than 1%, even in the best-case setting where $\delta = 1/2$ and $m = 1$. Moreover, as the bound on branch lengths m decreases, the distinguishability proportion further decreases, and is negligible when δ is close to zero or one.

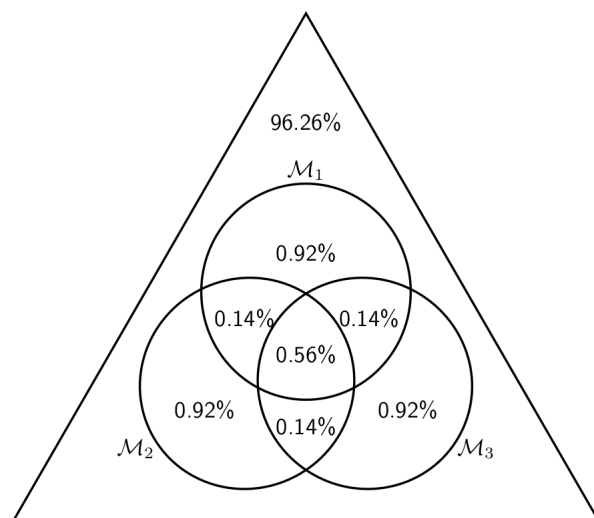


FIGURE 5. Venn diagram showing the percentage of points in Δ_4 which belong to the regions of intersections of the models $\mathcal{M}_1, \mathcal{M}_2$, and \mathcal{M}_3 . The vast majority of simplex points (96.2%) do not correspond to any of the three network models.

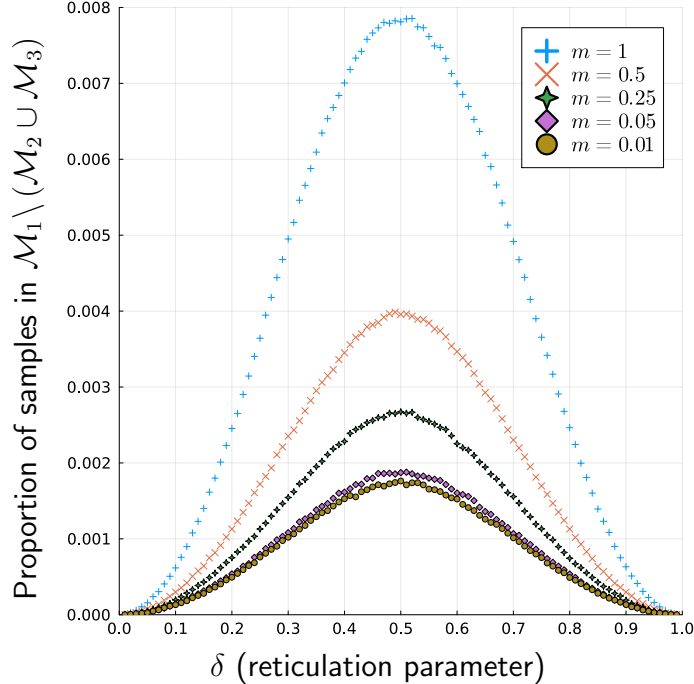


FIGURE 6. The proportion of networks in which the hybrid node is distinguishable as a function of δ , for \mathcal{N}_1 with branch lengths $t_1, \dots, t_6 \stackrel{iid}{\sim} \text{unif}(0, m)$.

3.5. Implications for Network Inference in Practice. The previous section shows that the three models overlap substantially, especially when considering biologically relevant parameters. Here we elaborate on some of the implications of the distinguishability criteria in Corollary 3.3 when taking into account additional biological considerations. We first start with an example to illustrate Corollary 3.3.

Example 3.6. Let \mathcal{N} be the 5-leaf network shown in Figure 7 and let X be a subset of the taxa $\{A, B, C, D, E\}$. Let $\mathcal{N}_{|X}$ be the restriction of \mathcal{N} to the taxa in X , $p_{|X}$ the site-pattern probability distribution from the Jukes-Cantor model on the restricted network when $\delta = \frac{1}{2}$, and $q_{|X}$ the image of $p_{|X}$ under the Fourier transform. Notice that when $|X| = 3$, $\mathcal{N}_{|X}$ is a tree unless X is equal to $\{A, B, C\}$, $\{A, B, E\}$, $\{A, C, D\}$, or $\{A, D, E\}$, in which case it is a 3-leaf triangle network.

As an example, consider the restriction of this network to the leaf set $\{A, C, D\}$. Matching the labels from Figure 3 to the version of the restricted network shown in Figure 8 (where A, C , and D match to 1, 2, and 3 respectively), we obtain the following values for the Fourier parameters:

$$\begin{aligned} a_1 &= e^{-\frac{4}{3}(.20)}, & a_2 &= e^{-\frac{4}{3}(.30)}, & a_3 &= e^{-\frac{4}{3}(.15)}, \\ a_4 &= e^{-\frac{4}{3}(.10)}, & a_5 &= e^{-\frac{4}{3}(.70)}, & a_6 &= e^{-\frac{4}{3}(.10)}. \end{aligned}$$

Substituting these values into the right-hand side of inequality (20) gives approximately 0.74, which is less than $a_1 \approx 0.77$. This tells us that $q_{\{A,C,D\}}$ could not have come from the 3-leaf triangle network where C is the leaf below the reticulation vertex. On the other hand, applying inequality (21) in a similar manner, we find the right hand side to be approximately 0.79, so the inequality is not satisfied. This tells us that $q_{\{A,C,D\}}$ could have come from a

3-leaf triangle network where D is the leaf below the reticulation vertex. As a result, it is *not* possible to determine the orientation of edges in the triangle of the 3-leaf network from $q_{\{A,C,D\}}$.

Applying the bounds for all of the triplets that result in 3-leaf triangle networks, we see that only when $X = \{A, D, E\}$ can we infer the orientation of edges in the triangle $\mathcal{N}_{|X}$ from $q_{|X}$. That we can identify the hybrid node in this example only for the two shortest leaf edges is in line with our observation from Example 1.1 that the signal of hybridization decays. Note that there is no way to gain distinguishability by adding additional leaves below the hybrid node, in contrast to the gene tree data setting (Allman et al., 2024).

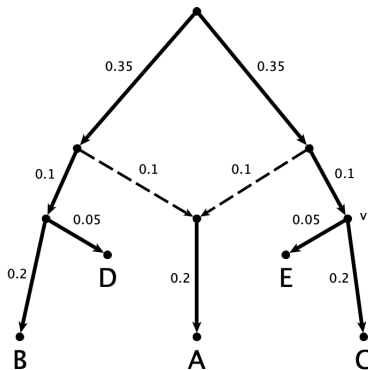


FIGURE 7. A 5-leaf network with branch lengths in expected number of mutations per site.

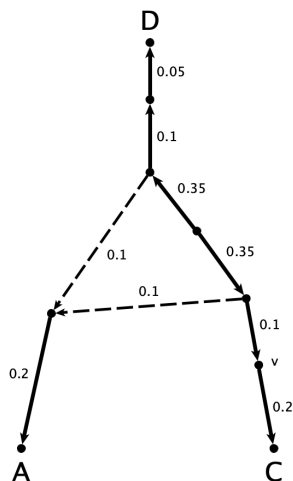


FIGURE 8. The network in Figure 7 restricted to $\{A, C, D\}$.

Careful interpretation of the inequalities in Corollary 3.3 suggests that the criteria for hybrid distinguishability are highly restrictive, even more so when biological considerations are taken into account. In particular, we find three necessary conditions for the hybrid node to be distinguishable.

First, the hybridization must be sufficiently recent. Inequalities (20) and (21) establish an exact age cutoff: if the hybridization is sufficiently ancient, i.e. $a_1 = e^{-4t_1/3}$ is sufficiently

small, then the hybrid node cannot be distinguished, even with unlimited data. Although this cutoff (the minimum of the right-hand sides of (20) and (21)) is a complicated function of the model parameters, it is not difficult to deduce the simpler necessary condition that distinguishability requires $a_1 > a_5$. Converting this condition to branch lengths, it holds that if the evolutionary distance t_1 between the initial hybrid and its present-day descendants is greater than the divergence t_5 between the hybrid’s parent species, then the hybrid will not be distinguishable.

Second, the evolutionary divergence between the parental species prior to hybridization must be sufficiently large for the hybrid to be distinguishable. If too little divergence took place prior to hybridization (i.e., if $a_5 = e^{-\frac{4}{3}t_5}$ is sufficiently close to 1), the right-hand sides of (20) and (21) exceed 1, in which case neither inequality can be satisfied since $a_1 < 1$. This requirement is restrictive because 3-cycles are expected to occur mostly between closely related taxa, as hybridization rates decline rapidly with evolutionary divergence (Mallet et al., 2007; Peñalba et al., 2024).

Third, distinguishability requires the hybrid’s descendants retain substantial minor-parent ancestry, i.e. from the parent species with the smaller genetic contribution to the hybrid. When the proportion of genomic material inherited from the minor-parent (i.e., $\min\{\delta, 1 - \delta\}$) is near zero, both inequalities (20) and (21) will fail because their right-hand sides exceed 1. This is illustrated in the plot of Figure 9, which shows that distinguishability is unlikely when δ is close to 0 or 1 (see Appendix C).

In practice, the required combination of high parental divergence together with substantial minor-parent ancestry is likely to be rare. Although F1 hybrids may exhibit $\delta \approx 1/2$, theoretical and empirical studies suggest that minor-parent ancestry typically decays rapidly through selective purging (within tens of generations) (Langdon et al., 2024; Moran et al., 2021; Veller et al., 2023). Thus, while retained levels of minor-parent ancestry exceeding 10% are not uncommon (Langdon et al., 2024; Moran et al., 2021), it is often the case that minor-parent ancestry is small, and this tends to be incompatible with distinguishability (see Figs. 6 and 9). This difficulty is compounded by the fact that selective purging is driven in part by hybrid incompatibilities, which increase nonlinearly with parental divergence (Langdon et al., 2024). Hence, the high parental divergence required for distinguishability is likely to coincide with *low* minor-parent ancestry, and this combination is likely to violate the distinguishability conditions.

Finally, we discuss the impact of the root location. The limitations of inferring the hybrid node in a 3-cycle can often, though not always, be circumvented through additional taxon sampling. If \mathcal{N}_1 is rooted on edge a_5 (as in Fig. 9), then adding an outgroup will result in a network with a 4-cycle, allowing for the use of tests based on 4-cycles. On the other hand, if the root lies on one of the leaf edges 2 or 3 (as shown in Fig. 10), this need not be possible. The network in Figure 10 could arise due to hybridization between two unsampled or extinct “ghost lineages” which both diverged from the ancestor of species 2 after its divergence with species 3. If species 3 is the closest extant relative of species 1 and 2, then additional taxon sampling will not yield a 4-cycle, so methods specific to 3-cycles are required.

However, in the ghost-lineage scenario in Figure 10, we expect the hybrid node to typically not be distinguishable from site pattern data, at least when approximately clock-like evolution is assumed. This is due to our next theorem, which shows that under a molecular clock model with all leaves equidistant from the root, the hybrid node will not be distinguishable.

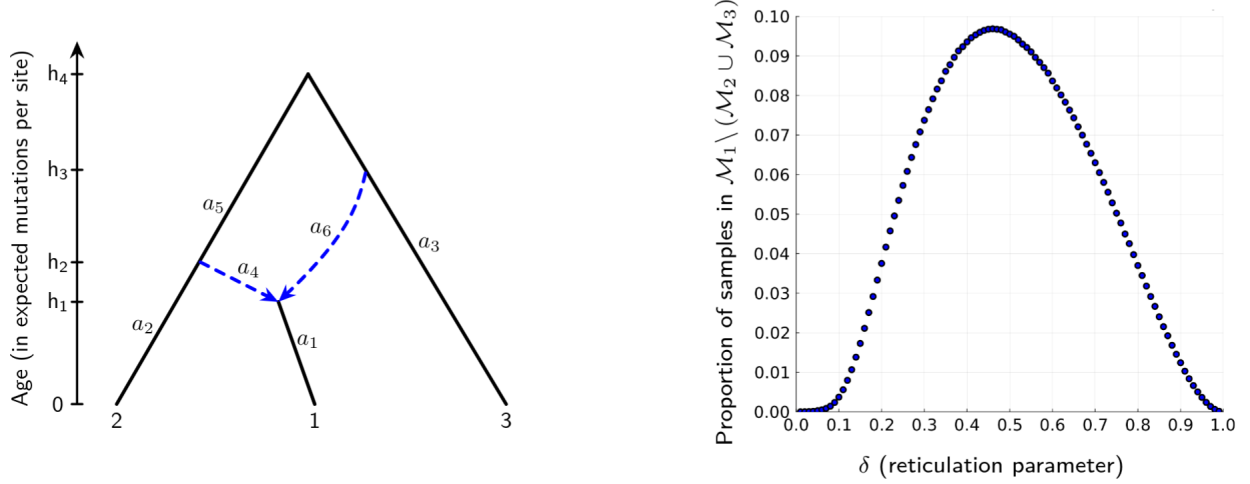


FIGURE 9. Left: The 3-leaf phylogenetic network \mathcal{N}_1 with root placed on the edge corresponding to the parameter a_5 . Right: The proportion of such networks for which the hybrid node is distinguishable, assuming the intervals $h_1, h_2 - h_1, h_3 - h_2$ and $h_4 - h_3$ are drawn uniformly at random from the interval $(0, .5)$. See Appendix C.

Theorem 3.7. *Under the ghost-lineage scenario shown in Figure 10 with the molecular clock assumption, for any choice of $0 < h_1 < h_2 < h_3 < h_4$, it holds that $\mathbf{q} \in \mathcal{M}_1 \cap \mathcal{M}_2$. In particular, the hybrid node in the 3-cycle is not distinguishable from the site pattern distribution.*

Proof. Let $h_1 < h_2 < h_3 < h_4$ be arbitrary. By the molecular clock assumption, the Fourier parameters are

$$(22) \quad \begin{aligned} a_1 &= e^{-\frac{4}{3}h_1} & a_2 &= e^{-\frac{4}{3}h_2} \\ a_3 &= e^{-\frac{4}{3}(2h_4-h_3)} & a_4 &= e^{-\frac{4}{3}(h_2-h_1)} \\ a_5 &= e^{-\frac{4}{3}(h_3-h_2)} & a_6 &= e^{-\frac{4}{3}(h_3-h_1)}. \end{aligned}$$

We need to show that $\mathbf{q} \in \mathcal{M}_1 \cap \mathcal{M}_2$. By Eq. (20) this occurs precisely when

$$\begin{aligned} & a_1(\delta a_4 a_5 + (1 - \delta)a_6)(\delta a_4(1 - a_3 a_5) + (1 - \delta)a_5 a_6(1 - a_3)) \\ & < a_5(\delta a_4(1 - a_3 a_5) + (1 - \delta)a_6(1 - a_3)). \end{aligned}$$

By Eq. (22), the Fourier parameters satisfy $a_2 = a_1 a_4$ and $a_6 = a_4 a_5$. Using these relations, the above inequality can be rewritten (code available in the supplemental materials in the file `ghost-scenario-calculation.m2`) as

$$\begin{aligned} & a_6(a_2 a_3 a_5^2 \delta - a_2 a_3 a_5^2 - a_2 a_3 a_5 \delta - a_2 a_5^2 \delta \\ & + a_2 a_5^2 + a_2 \delta + a_3 a_5 + a_5 \delta - a_5 - \delta) < 0. \end{aligned}$$

The left-hand side factors as

$$-a_6[\delta(1 - a_2)(1 - a_3 a_5) + (1 - \delta)a_5(1 - a_3)(1 - a_2 a_5)],$$

which is clearly negative for all $a_2, a_3, a_5, a_6, \delta \in (0, 1)$. Hence $\mathbf{q} \in \mathcal{M}_1 \cap \mathcal{M}_2$. \square

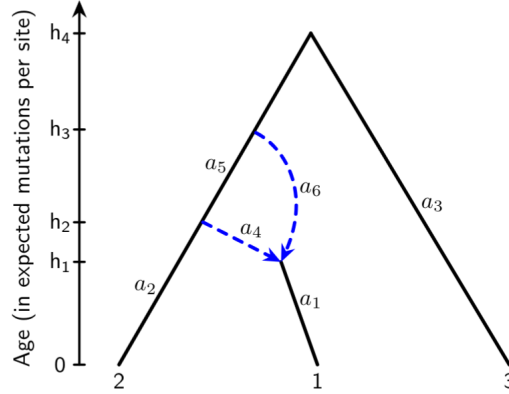


FIGURE 10. A 3-leaf phylogenetic network rooted on edge 3 at time h_4 . The network exhibits a 3-cycle arising from ghost lineages that diverged from species 2 at times h_3 and h_2 and later hybridized at time h_1 . Note that a_3 is the Fourier parameter of leaf 3 when the root is suppressed.

3.6. Applications to Biological Data. In this section, we present two examples from the literature where a phylogenetic network is inferred from biological data. We restrict these networks to a subset of the taxa so that the inferred networks are triangle networks. We then apply the bound from Corollary 3.3 to determine if the inferred parameters are identifiable under the Jukes-Cantor model. Our goal in this section is simply to give insight into the implications of our results for practical inference. As such, we have derived parameter values from the published literature that are likely of interest to biologists. But, we note that networks were not inferred assuming that the data were generated by the Jukes-Cantor network models we study.

3.6.1. *Melinaea*. In (van der Heijden et al., 2025), the authors study the lineages of *Melinaea* and *Mechanitis* butterflies found throughout Central and South America and provide evidence of fast and recent radiation. Here, we examine one of the triangle networks from that paper involving *Melinaea idae*, *Melinaea lilis*, and *Melinaea marsaeus*. *Mel. idae* and *Mel. lilis* are sister species while *Mel. marsaeus* is a representative of the ingroup clade involved in the study. The authors fit the network using the multispecies-coalescent-with-introgression (MSCi) model implemented in BPP v.4.6.2 (Flouri et al., 2019). For their analysis, they assumed a mutation rate of 2.9×10^{-9} substitutions per site per generation and four generations per year. Converting the branch lengths from scenario 1 of the inferred species network in (van der Heijden et al., 2025, Fig. 3A) into expected number of substitutions per site, we obtain the network shown in Figure 11.

After converting the branch lengths to Fourier parameters, we then substituted them (and the estimate $\delta = .261$) into the right-hand sides of the inequalities in Corollary 3.3. This gave ≈ 1.0004 for (20) and ≈ 1.0003 for (21), both of which are greater than $a_1 = .997$. Hence, neither inequality is satisfied, and therefore the hybrid is *not* distinguishable. Together, these results imply that under the Jukes-Cantor model with no coalescence, any of the three species could be the hybrid descendant.

3.6.2. *Rhizoplaca*. In (Keuler et al., 2020), the authors use maximum pseudolikelihood, implemented in PhyloNet (Wen et al., 2018), to obtain a phylogenetic network for seven lichenized fungus species in the genus *Rhizoplaca*. We replicate their analysis without bootstrap

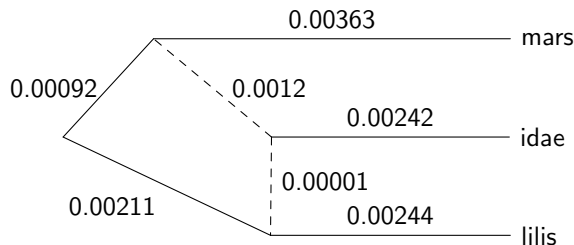


FIGURE 11. Network from van der Heijden et al. (2025) on three species of neotropical butterflies with branch lengths converted to expected number of mutations per site.

thresholding, while constraining the number of hybridizations to one. Our code is available in the supplemental materials in `src/rhizoplaca/`. The top-scoring network is shown in Figure 12; branch lengths were converted from coalescent units to expected number of mutations per site using the population mutation parameter $\theta = 2 \times 10^{-3}$, which roughly accords with estimates found by Leavitt et al. (2013). This network appears to closely match the network obtained in (Keuler et al., 2020, Fig. 4(a)), which does not include branch lengths for the leaf edges and reticulation edges since it was inferred from gene tree topologies.

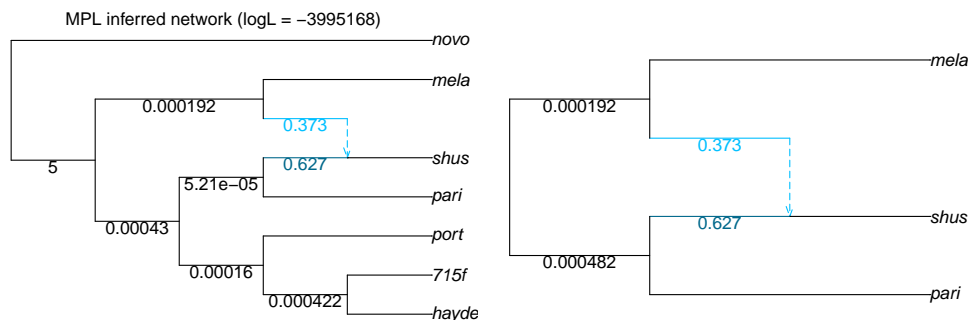


FIGURE 12. The highest-scoring phylogenetic network for *Rhizoplaca* with one reticulation, with internal branch lengths expressed in expected number of mutations per site, and its restriction to a 3-taxon network.

If we restrict the network to the leaves labeled *mela*, *pari*, and *shus*, we obtain the rooted 3-cycle network with *shus* the hybrid species (see Fig. 12). Following Example 1.1, let us suppose that the leaf edges all have branch length s , measured in expected number of mutations per site, and that the reticulation edges are of negligible length. Using the bound in Corollary 3.3, we find that it is possible to determine the direction of hybridization, i.e., that *shus* is the hybrid descendant, if and only if the evolutionary distance s is less than approximately 0.00017 expected mutations per site.

4. DISCUSSION

Since hybridization in eukaryotes occurs most commonly between closely-related taxa (Mallet et al., 2016), 3-cycles are likely to be common in nature; however, they have posed significant challenges from an identifiability standpoint. Due to these challenges, previous

identifiability results have routinely excluded networks with 3-cycles from consideration, leaving a gap in the literature.

In this work, we fully describe the semialgebraic sets of the Fourier transformed distributions that arise from each of the three 3-leaf triangle networks under the Jukes-Cantor model of DNA substitution. Furthermore, for each pair of 3-leaf triangle networks, we give an explicit semialgebraic description of the set of parameters of the first model that gets mapped into the intersection of both models; this set of parameters constitutes approximately 92.8% of the numerical parameter space $\Theta_{\mathcal{M}_1} \times (0, 1)$. Thus, the primary conclusion is that there is a full-dimensional region in the space of site-pattern probabilities where identifying the hybrid node is possible, and a full-dimensional region where identifying the hybrid node is impossible, even with infinitely long sequences.

Further analysis of our results from a practical lens suggests that it is generally not possible to determine the orientation of edges in a 3-leaf triangle network using the site pattern distribution. Hybrid distinguishability requires recent hybridization, high parental divergence, and substantial minor-parent ancestry, conditions which are unlikely to all be satisfied, especially simultaneously. These results are consistent with the intuition that the signal distinguishing the hybrid lineage is expected to be weakest when hybridization took place a long time ago, or between closely-related taxa. What is more surprising is our conclusion, highlighted in Example 1.1, that this loss of identifiability is subject to a sharp cutoff.

This paper focuses solely on the Jukes-Cantor model, however, we expect that similar techniques can be used for other group-based models, such as the Kimura 2-parameter (K2P) and Kimura 3-parameter (K3P) models. The Jukes-Cantor model is a sub-model of both of these, obtained by identifying certain entries in the Markov transition matrices. From the model perspective, the Jukes-Cantor model for a network can be obtained by intersecting the K2P or K3P model for that network with a linear space. While our work suggests that similar results might hold for these other models, it is not clear that any are immediately implied by this work. Thus, it may be the case that hybrid node identification is more plausible under these different models.

Likewise, the network-based models we study, if we assume ultrametricity, can be seen as a limit of the network multispecies coalescent (NMSC) model as population sizes approach zero. Similar identifiability results have also been established for the NMSC model using semialgebraic conditions. Allman et al. (2024) show that in level-1 networks, 3-cycles generally can be detected from gene tree quartet concordance factors under the NMSC model. In addition, they show that the location of the hybrid node in the 3-cycle can sometimes be determined and sometimes not, depending on the numerical parameters, the number of leaves, and their position relative to the hybrid node. Although the results in (Allman et al., 2024) do not imply the results presented in this paper (see Remark 4.7 in (Allman et al., 2024)), there are parallels between their results and those of this paper. The precise nature of this connection is not well-understood as the results are based on fundamentally different data types. A related question, and an especially important one for applications, is to understand under what conditions 3-cycles can be inferred assuming a model combining both coalescence and substitution (e.g. see Allman et al. (2022)).

We have shown that the inequalities of Theorem 3.1 contain important information about model membership. This naturally suggests that it may be possible to use these inequalities for network inference, in very restrictive settings, using techniques designed for models described by algebraic constraints, for example, by using incomplete U-statistics (Barnhill

et al., 2025; Sturma et al., 2024) or by substituting sequence data into the defining polynomial equalities and inequalities and using scoring or supervised machine learning algorithms for inference (Barton et al., 2026; Casanellas et al., 2021; Martin et al., 2025). However, the results of this paper point to an important caution in the development of such classification algorithms. In particular, these algorithms should take into account that the space of expected site pattern frequencies contains substantial regions where the classification problem does not have a unique solution. On the other hand, the results of this paper establish that classification is theoretically possible over very specific parameter regimes.

Finally, we emphasize that the results of this work should not be interpreted as settling the question of indistinguishability of 3-cycles more broadly. Rather, as discussed above, our conclusions are restricted to the problem of inferring hybrid nodes from site-pattern frequency distributions under the Jukes–Cantor substitution model. Other sources of genetic signal, including synteny and gene tree discordance, may provide substantially stronger information for reconstructing 3-cycles.

ACKNOWLEDGMENTS

This research began during the Fall 2025 Graduate Research Community at the University of Hawai'i at Mānoa supported by the National Science Foundation (DGE-2429967). AE was additionally supported by NSF Award DMS-2023239. EG was additionally supported by DMS-2527518.

SUPPLEMENTARY MATERIALS

Supplementary materials can be found in the following GitHub repository: <https://github.com/max-hill/semialgebraic-conditions-for-triangle-networks>.

REFERENCES

- Allman, E. S., C. Ané, H. Baños, and J. A. Rhodes. 2025. Beyond level-1: Identifiability of a class of galled tree-child networks. arXiv:2504.21116.
- Allman, E. S., H. Baños, M. Garrote-Lopez, and J. A. Rhodes. 2024. Identifiability of level-1 species networks from gene tree quartets. *Bull. Math. Biol.* 86:110.
- Allman, E. S., H. Baños, and J. A. Rhodes. 2022. Identifiability of species network topologies from genomic sequences using the logDet distance. *J. Math. Biol.* 84:35.
- Baños, H. 2019. Identifying species network features from gene tree quartets under the coalescent model. *Bull. Math. Biol.* 81:494–534.
- Barley, A. J., A. Nieto-Montes de Oca, N. L. Manríquez-Morán, and R. C. Thomson. 2022. The evolutionary network of whiptail lizards reveals predictable outcomes of hybridization. *Science* 377:773–777.
- Barnhill, D., M. Garrote-López, E. Gross, M. Hill, B. Kagy, J. A. Rhodes, and J. Z. Zhang. 2025. Methodological considerations for semialgebraic hypothesis testing with incomplete U-statistics. arXiv:2507.13531 .
- Barton, T., E. Gross, C. Long, and J. Rusinko. 2026. Statistical learning with phylogenetic network invariants. *Bull. Soc. Syst. Biol.* 4 no. 1 (2026) 4.
- Casanellas, M., J. Fernández-Sánchez, and M. Garrote-López. 2021. SAQ: Semi-algebraic quartet reconstruction. *IEEE/ACM Trans. Comput. Biol. Bioinform.* 18:2855–2861.
- Cui, R., M. Schumer, K. Kruesi, R. Walter, P. Andolfatto, and G. G. Rosenthal. 2013. Phylogenomics reveals extensive reticulate evolution in Xiphophorus fishes. *Evolution* 67:2166–2179.
- Englander, A. K., M. Frohn, E. Gross, N. Holtgreffe, L. van Iersel, M. Jones, and S. Sullivant. 2025. Identifiability of phylogenetic level-2 networks under the Jukes-Cantor model. bioRxiv Pages 2025–04.
- Evans, S. N. and T. P. Speed. 1993. Invariants of some probability models used in phylogenetic inference. *Ann. Stat.* Pages 355–377.
- Flouri, T., X. Jiao, B. Rannala, and Z. Yang. 2019. A Bayesian implementation of the multispecies coalescent model with introgression for phylogenomic analysis. *Mol. Biol. Evol.* 37.
- Gambette, P., K. T. Huber, and S. Kelk. 2017. On the challenge of reconstructing level-1 phylogenetic networks from triplets and clusters. *J. Math. Biol.* 74:1729–1751.
- Gross, E. and C. Long. 2018. Distinguishing phylogenetic networks. *SIAM J. Appl. Algebra Geom.* 2:72–93.
- Gross, E., L. van Iersel, R. Janssen, M. Jones, C. Long, and Y. Murakami. 2021. Distinguishing level-1 phylogenetic networks on the basis of data generated by Markov processes. *J. Math. Biol.* 83:1–24.
- Hibbins, M. S. and M. W. Hahn. 2022. Phylogenomic approaches to detecting and characterizing introgression. *Genetics* 220:iyab173.
- Holtgreffe, N., E. S. Allman, H. Baños, L. van Iersel, V. Moulton, J. A. Rhodes, and K. Wicke. 2025. Distinguishing phylogenetic level-2 networks with quartets and inter-taxon quartet distances. arXiv:2507.17308.
- Jukes, T. H., C. R. Cantor, et al. 1969. Evolution of protein molecules. *Mammalian protein metabolism* 3:132.
- Keuler, R., A. Garretson, T. Saunders, R. J. Erickson, N. St. Andre, F. Grewe, H. Smith, H. T. Lumbsch, J.-P. Huang, L. L. St. Clair, and S. D. Leavitt. 2020. Genome-scale data

- reveal the role of hybridization in lichen-forming fungi. *Sci. Rep.* 10:1497.
- Krantz, S. and H. Parks. 2008. *Geometric integration theory*. Springer.
- Langdon, Q. K., J. S. Groh, S. M. Aguillon, D. L. Powell, T. Gunn, C. Payne, J. J. Baczenas, A. Donny, T. O. Dodge, K. Du, et al. 2024. Swordtail fish hybrids reveal that genome evolution is surprisingly predictable after initial hybridization. *PLoS Biology* 22:e3002742.
- Leavitt, S. D., F. Fernández-Mendoza, S. Pérez-Ortega, M. Sohrabi, P. K. Divakar, J. Vondrák, H. Thorsten Lumbsch, and L. L. S. Clair. 2013. Local representation of global diversity in a cosmopolitan lichen-forming fungal species complex (Rhizoplaca, Ascomycota). *J. Biogeogr.* 40:1792–1806.
- Mallet, J. 2005. Hybridization as an invasion of the genome. *Trends Ecol. Evol.* 20:229–237.
- Mallet, J., M. Beltrán, W. Neukirchen, and M. Linares. 2007. Natural hybridization in heliconiine butterflies: the species boundary as a continuum. *BMC Evol. Biol.* 7:28.
- Mallet, J., N. Besansky, and M. W. Hahn. 2016. How reticulated are species? *BioEssays* 38:140–149.
- Martin, S., N. Holtgreffe, V. Moulton, and R. M. Leggett. 2025. Algebraic invariants for inferring 4-leaf semi-directed phylogenetic networks. *Syst. Biol.* Page syaf071.
- Moran, B. M., C. Payne, Q. Langdon, D. L. Powell, Y. Brandvain, and M. Schumer. 2021. The genomic consequences of hybridization. *Elife* 10:e69016.
- Pardi, F. and C. Scornavacca. 2015. Reconstructible phylogenetic networks: do not distinguish the indistinguishable. *PLoS Comput. Biol.* 11:e1004135.
- Peñalba, J. V., A. Runemark, J. I. Meier, P. Singh, G. O. Wogan, R. Sánchez-Guillén, J. Mallet, S. J. Rometsch, M. Menon, O. Seehausen, et al. 2024. The role of hybridization in species formation and persistence. *Cold Spring Harb. Perspect. Biol.* 16:a041445.
- Rhodes, J. A., H. Baños, J. Xu, and C. Ané. 2025. Identifying circular orders for blobs in phylogenetic networks. *Adv. Appl. Math.* 163:102804.
- Rose, J. P., B. Li, M. J. Sporck-Koehler, E. A. Stacy, K. R. Wood, E. M. Lemmon, A. R. Lemmon, C. Ané, K. J. Sytsma, and T. J. Givnish. 2025. Phylogenomics of the tetraploid Hawaiian lobeliads: Implications for their origin, dispersal history, and adaptive radiation. *Proc. Natl. Acad. Sci. U.S.A.* 122:e2421004122.
- Semple, C., M. Steel, et al. 2003. *Phylogenetics* vol. 24. Oxford University Press.
- Solís-Lemus, C. and C. Ané. 2016. Inferring phylogenetic networks with maximum pseudo-likelihood under incomplete lineage sorting. *PLoS Genet.* 12:e1005896.
- Sturma, N., M. Drton, and D. Leung. 2024. Testing many constraints in possibly irregular models using incomplete U-statistics. *J. R. Stat. Soc. Ser. B Stat Methodol.* 86:987–1012.
- Sturmfels, B. and S. Sullivant. 2005. Toric ideals of phylogenetic invariants. *J. Comput. Biol.* 12:457–481.
- Sullivant, S. 2023. *Algebraic Statistics* vol. 194. AMS.
- The algebraic-phylogenetics collaboration. 2026. A database of small trees and networks in algebraic phylogenetics. Version 0.3. Available at <http://www.algebraicphylogenetics.org>.
- van der Heijden, E. S. M., K. Näsvall, F. A. Seixas, C. E. B. Nobre, A. C. D. Maia, P. Salazar-Carrión, J. M. Walker, D. Szczerbowski, S. Schulz, I. A. Warren, K. G. G. Córdova, M. J. Sánchez-Carvajal, F. Chandi, A. P. Arias-Cruz, N. Rueda-M, C. Salazar, K. K. Dasmahapatra, S. H. Montgomery, M. McClure, D. E. Absolon, T. C. Mathers, C. A. Santos, S. McCarthy, J. M. D. Wood, G. Lamas, C. Bacquet, A. V. L. Freitas, K. R. Willmott, C. D. Jiggins, M. Elias, and J. I. Meier. 2025. Genomics of neotropical biodiversity indicators:

- Two butterfly radiations with rampant chromosomal rearrangements and hybridization. *Proc. Natl. Acad. Sci. U.S.A.* 122:e2410939122.
- Veller, C., N. B. Edelman, P. Muralidhar, and M. A. Nowak. 2023. Recombination and selection against introgressed DNA. *Evolution* 77:1131–1144.
- Wen, D., Y. Yu, J. Zhu, and L. Nakhleh. 2018. Inferring phylogenetic networks using PhyloNet. *Syst. Biol.* 67:735–740.
- Xu, J. and C. Ané. 2023. Identifiability of local and global features of phylogenetic networks from average distances. *J. Math. Biol.* 86:12.
- Zhang, C., H. A. Ogilvie, A. J. Drummond, and T. Stadler. 2018. Bayesian inference of species networks from multilocus sequence data. *Mol. Biol. Evol.* 35:504–517.

APPENDIX A. PROOF OF THEOREM 3.1

We begin by introducing a reparameterization which will simplify our analysis. We substitute $a_4^* := \delta a_1 a_4$ and $a_6^* := (1 - \delta) a_1 a_6$ where the new parameters $a_4^*, a_6^* \in (0, 1)$ and must satisfy $a_4^* + a_6^* < 1$, but are otherwise free. In these new parameters (omitting the stars to simplify notation), we now have:

$$(23) \quad \mathcal{M}_1 : \begin{array}{ll} q_{\text{ACC}} = a_2 a_3 a_5 & q_{\text{CAC}} = a_3 a_4 a_5 + a_3 a_6 \\ q_{\text{CCA}} = a_2 a_4 + a_2 a_5 a_6 & q_{\text{CGT}} = a_2 a_3 a_5 (a_4 + a_6). \end{array}$$

The corresponding parameter space for network \mathcal{N}_1 is

$$\tilde{\Theta}_{\mathcal{N}_1} = \{(a_2, a_3, a_4, a_5, a_6) : 0 < a_2, a_3, a_4, a_5, a_6 < 1 \text{ and } a_4 + a_6 < 1\} \subseteq \mathbb{R}^5.$$

We will use $\tilde{\psi}_{\mathcal{N}_1}$ to denote the new parameterization map shown in Eq. (23). With this new notation

$$\mathcal{M}_1 = \{\tilde{\psi}_{\mathcal{N}_1}(\theta) : \theta \in \tilde{\Theta}_{\mathcal{N}_1}\}.$$

Similar simplifications give reparameterizations for the other two networks \mathcal{N}_2 and \mathcal{N}_3 shown in Figure 3, which are as follows:

$$\mathcal{M}_2 : \begin{array}{ll} q_{\text{ACC}} = b_3 b_4 b_5 + b_3 b_6 & q_{\text{CAC}} = b_1 b_3 b_5 \\ q_{\text{CCA}} = b_1 b_4 + b_1 b_5 b_6 & q_{\text{CGT}} = b_1 b_3 b_5 (b_4 + b_6) \end{array}$$

$$\mathcal{M}_3 : \begin{array}{ll} q_{\text{ACC}} = c_2 c_4 c_5 + c_2 c_6 & q_{\text{CAC}} = c_1 c_4 + c_1 c_5 c_6 \\ q_{\text{CCA}} = c_1 c_2 c_5 & q_{\text{CGT}} = c_1 c_2 c_5 (c_4 + c_6). \end{array}$$

We now prove Theorem 3.1, which provides a complete semialgebraic description of \mathcal{M}_1 . We present the proof of this theorem in the following two subsections. In particular, the equivalence statement in the theorem will follow immediately from Lemmas A.1 and A.4, and the additional inequalities (13), (14), and (15) will follow from Lemma A.2.

A.1. Proof of the ‘‘Only If’’ Direction of Theorem 3.1. Our first lemma establishes the forward direction of Theorem 3.1.

Lemma A.1. *If $(q_{\text{ACC}}, q_{\text{CAC}}, q_{\text{CCA}}, q_{\text{CGT}}) \in \mathcal{M}_1$ then inequalities (8), (9), (10), (11), and (12) hold.*

Proof. By definition of \mathcal{M}_1 , there exists $(a_2, \dots, a_6) \in (0, 1)^5$ with $a_4 + a_6 < 1$ such that

$$\tilde{\psi}_{\mathcal{N}_1}(a_2, a_3, a_4, a_5, a_6) = (q_{\text{ACC}}, q_{\text{CAC}}, q_{\text{CCA}}, q_{\text{CGT}}).$$

Therefore, $q_{\text{ACC}}, q_{\text{CAC}}, q_{\text{CCA}}$, and q_{CGT} are given by the formulas in Eq. (23), which we will use to prove inequalities (8), (9), (10), (11), and (12).

We begin by proving inequality (8). By the formulas in Eq. (23), it is easily seen that $q_{\text{ACC}}, q_{\text{CAC}}, q_{\text{CCA}}, q_{\text{CGT}} > 0$ since $a_2, a_3, a_4, a_5, a_6 > 0$. It is also clear that $q_{\text{ACC}}, q_{\text{CGT}} < 1$ since $a_2, a_3, a_4, a_5, a_6 < 1$ and $a_4 + a_6 < 1$. It remains to show that $q_{\text{CAC}} < 1$ and $q_{\text{CCA}} < 1$. Since the two are similar, we show only the case of q_{CAC} , which proceeds as follows:

$$\begin{aligned} q_{\text{CAC}} &= a_3 a_4 a_5 + a_3 a_6 \\ &= a_3 (a_4 a_5 + a_6) \\ &< a_3 (a_4 + a_6) && \text{since } a_5 < 1 \\ &< 1, \end{aligned}$$

where the last inequality is due to $a_3 < 1$ and $a_4 + a_6 < 1$.

Next we will prove inequality (9). By definition of $\tilde{\psi}_{\mathcal{N}_1}$,

$$\begin{aligned} q_{\text{ACC}} - q_{\text{CGT}} &= a_2 a_3 a_5 - (a_2 a_3 a_4 a_5 + a_2 a_3 a_5 a_6) \\ &= a_2 a_3 a_5 (1 - (a_4 + a_6)) \\ &> 0, \end{aligned}$$

where the last inequality follows due to $a_2, a_3, a_5 > 0$ and $a_4 + a_6 < 1$.

To prove inequality (10), first observe that the formulas in Eq. (23) imply

$$\begin{aligned} q_{\text{CGT}} - q_{\text{ACC}} q_{\text{CAC}} &= a_2 a_3 a_5 (a_4 + a_6) - a_2 a_3^2 a_5 (a_4 a_5 + a_6) \\ &= a_2 a_3 a_5 (a_4 (1 - a_3 a_5) + a_6 (1 - a_3)). \end{aligned}$$

Again, this must be greater than 0 since $a_2, a_3, a_4, a_5, a_6 > 0$ and $a_3, a_5 < 1$.

Inequality (11) was first shown in Englander et al. (2025); the proof presented here is essentially the same as theirs: substituting in the formulas from Eq. (23) and rearranging terms, one finds that

$$(24) \quad q_{\text{ACC}} q_{\text{CAC}} q_{\text{CCA}} - q_{\text{CGT}}^2 = a_2^2 a_3^2 a_4 a_5 a_6 (1 - a_5)^2,$$

which is positive since $a_4, a_5, a_6 > 0$ and $a_5 < 1$.

Finally, to prove inequality (12), observe that by Eq. (23), the left hand side of (12) can be written as

$$a_2 a_3 a_5 (a_4 (1 - a_2) (1 - a_3 a_5) + a_6 (1 - a_3) (1 - a_2 a_5)),$$

which is positive since $a_2, a_3, a_4, a_5, a_6 > 0$ and $a_2, a_3, a_5 < 1$. □

Lemma A.2 (Additional inequalities). *If $(q_{\text{ACC}}, q_{\text{CAC}}, q_{\text{CCA}}, q_{\text{CGT}}) \in \mathcal{M}_1$, then*

$$(13) \quad q_{\text{CAC}} - q_{\text{CGT}} > 0$$

$$(14) \quad q_{\text{CCA}} - q_{\text{CGT}} > 0$$

$$(15) \quad q_{\text{CGT}} - q_{\text{ACC}} q_{\text{CCA}} > 0$$

Proof. Using the formulas from Eq. (23), it is easily verified that the three inequalities may be written as

$$\begin{aligned} q_{\text{CAC}} - q_{\text{CGT}} &= a_3 [a_4 a_5 (1 - a_2) + a_6 (1 - a_2 a_5)] \\ q_{\text{CCA}} - q_{\text{CGT}} &= a_2 [a_4 (1 - a_3 a_5) + a_5 a_6 (1 - a_3)] \\ q_{\text{CGT}} - q_{\text{ACC}} q_{\text{CCA}} &= a_2 a_3 a_5 [a_4 (1 - a_2) + a_6 (1 - a_2 a_5)]. \end{aligned}$$

In all three cases, the right hand sides are seen to be positive by inspection, since $0 < a_2, a_3, a_4, a_5, a_6 < 1$. □

A.2. Proof of the “If” Direction of Theorem 3.1. In this section we prove the backwards direction of Theorem 3.1. Namely, we will show that if $q_{\text{ACC}}, q_{\text{CAC}}, q_{\text{CCA}}$, and q_{CGT} satisfy inequalities (8), (9), (10), (11), and (12), then there exists $(a_2, a_3, a_4, a_5, a_6) \in \tilde{\Theta}_{\mathcal{N}_1}$ such that $\tilde{\psi}_{\mathcal{N}_1}(a_2, a_3, a_4, a_5, a_6) = (q_{\text{ACC}}, q_{\text{CAC}}, q_{\text{CCA}}, q_{\text{CGT}})$.

We begin by showing that for any $\mathbf{q} = (q_{\text{ACC}}, q_{\text{CAC}}, q_{\text{CCA}}, q_{\text{CGT}}) \in \mathbb{R}^4$ satisfying inequality (11), the fiber $\tilde{\psi}_{\mathcal{N}_1}^{-1}(\mathbf{q})$ contains a one-dimensional family of points in \mathbb{R}^5 parameterized by a single free parameter.

Lemma A.3 (Existence of a one-parameter real family of solutions). *Assume that the coordinates $(q_{\text{ACC}}, q_{\text{CAC}}, q_{\text{CCA}}, q_{\text{CGT}}) \in \mathbb{R}^4$ satisfy inequality (11). Then there exists a family of solutions in \mathbb{R}^5 to the polynomial system*

$$(25) \quad \begin{cases} q_{\text{ACC}} = a_2 a_3 a_5 \\ q_{\text{CAC}} = a_3 a_4 a_5 + a_3 a_6 \\ q_{\text{CCA}} = a_2 a_4 + a_2 a_5 a_6 \\ q_{\text{CGT}} = a_2 a_3 a_4 a_5 + a_2 a_3 a_5 a_6 \end{cases}$$

taking the form $(a_2, a_3, a_4, a_5, a_6) \in \mathbb{R}^5$, where $a_2 \in \mathbb{R} \setminus \{0\}$ is a free variable and

$$(26) \quad a_3 = \frac{q_{\text{ACC}} q_{\text{CAC}} a_2 - q_{\text{ACC}} q_{\text{CGT}}}{q_{\text{CGT}} a_2 - q_{\text{ACC}} q_{\text{CCA}}}$$

$$(27) \quad a_4 = \frac{a_2 u}{q_{\text{ACC}} q_{\text{CAC}} a_2^2 - 2 q_{\text{ACC}} q_{\text{CGT}} a_2 + q_{\text{ACC}}^2 q_{\text{CCA}}}$$

$$(28) \quad a_5 = \frac{q_{\text{CGT}} a_2 - q_{\text{ACC}} q_{\text{CCA}}}{q_{\text{CAC}} a_2^2 - q_{\text{CGT}} a_2}$$

$$(29) \quad a_6 = \frac{(q_{\text{CAC}} a_2 - q_{\text{CGT}})(q_{\text{CGT}} a_2 - q_{\text{ACC}} q_{\text{CCA}})}{q_{\text{ACC}} q_{\text{CAC}} a_2^2 - 2 q_{\text{ACC}} q_{\text{CGT}} a_2 + q_{\text{ACC}}^2 q_{\text{CCA}}},$$

where $u = q_{\text{ACC}} q_{\text{CAC}} q_{\text{CCA}} - q_{\text{CGT}}^2$.

Proof. The computations to verify that equations Eq. (26)-(29) yield symbolic solutions to (25) can be found in the file `one-param-family-computation.m2` in the Supplementary Materials. It remains only to show that the denominators of Eq. (26)-(29) are non-zero for all $a_2 \in \mathbb{R} \setminus \{0\}$.

We first note that since we assume inequality (11), any solution of the polynomial system 25 must satisfy $a_2, a_3, a_4, a_5, a_6 \neq 0$ and $a_5 \neq 1$, which follows immediately by inspection of Eq. (24).

To see that the denominators of Eqs. (26) and (28) are nonzero, we write them in terms of the Fourier parameters as follows:

$$q_{\text{CGT}} a_2 - q_{\text{ACC}} q_{\text{CCA}} = a_2^2 a_3 a_5 a_6 (1 - a_5).$$

and

$$q_{\text{CAC}} a_2^2 - q_{\text{CGT}} a_2 = a_2^2 a_3 a_6 (1 - a_5).$$

Both of these are nonzero since $a_2, a_3, a_5, a_6 \neq 0$ and $a_5 \neq 1$.

Finally, observe that the denominator of Eqs. (27) and (29) is quadratic in the variable a_2 . The discriminant is

$$4 q_{\text{ACC}}^2 (q_{\text{CGT}}^2 - q_{\text{ACC}} q_{\text{CAC}} q_{\text{CCA}}),$$

or equivalently, since $q_{\text{ACC}} = a_2 a_3 a_5$,

$$4 (a_2 a_3 a_5)^2 (q_{\text{CGT}}^2 - q_{\text{ACC}} q_{\text{CAC}} q_{\text{CCA}}).$$

This is negative by inequality (11), and hence the quadratic is nonzero for all $a_2 \in \mathbb{R} \setminus \{0\}$. \square

The next lemma establishes the backwards direction of Theorem 3.1.

Lemma A.4. *If $(q_{\text{ACC}}, q_{\text{CAC}}, q_{\text{CCA}}, q_{\text{CGT}}) \in \mathbb{R}^4$ satisfies inequalities (8), (9), (10), (11), and (12), then $(q_{\text{ACC}}, q_{\text{CAC}}, q_{\text{CCA}}, q_{\text{CGT}}) \in \mathcal{M}_1$.*

Proof. By definition of \mathcal{M}_1 , we need to show there exists a solution $(a_2, a_3, a_4, a_5, a_6)$ to the polynomial system (25) satisfying $0 < a_2, a_3, a_4, a_5, a_6 < 1$ and $a_4 + a_6 < 1$.

Assume a_3, a_4, a_5, a_6 are given by Eqs. (26) to (29), with a_2 to be chosen later. By Lemma A.3, it will suffice to show that there exists $a_2 \in (0, 1)$ such that $0 < a_3, a_4, a_5, a_6 < 1$ and $a_4 + a_6 < 1$. Let

$$\eta := \frac{q_{\text{ACC}}(q_{\text{CCA}} - q_{\text{CGT}})}{q_{\text{CGT}} - q_{\text{ACC}}q_{\text{CAC}}}.$$

We will show that $\eta \in (0, 1)$, and that $0 < a_3, a_4, a_5, a_6 < 1$ and $a_4 + a_6 < 1$ whenever $\eta < a_2 < 1$. The proof proceeds through a series of claims. Our first claim presents a series of useful inequalities which, among other things, will verify that $\eta \in (0, 1)$.

Claim 1: $0 < \frac{q_{\text{CGT}}}{q_{\text{CAC}}} < \frac{q_{\text{ACC}}q_{\text{CCA}}}{q_{\text{CGT}}} < \eta < 1$.

Proof of Claim 1. We prove the inequalities from left to right. The first inequality follows trivially by the assumption that $q_{\text{CGT}}, q_{\text{CAC}} > 0$, and the second follows directly by inequality (11).

To prove the third inequality, observe that $q_{\text{ACC}}q_{\text{CAC}}q_{\text{CCA}} > q_{\text{CGT}}^2$ by inequality (11). Multiplying by $-q_{\text{ACC}}$ and then adding $q_{\text{ACC}}q_{\text{CCA}}q_{\text{CGT}}$ to both sides yields

$$q_{\text{ACC}}q_{\text{CCA}}q_{\text{CGT}} - q_{\text{ACC}}^2q_{\text{CAC}}q_{\text{CCA}} < q_{\text{ACC}}q_{\text{CCA}}q_{\text{CGT}} - q_{\text{ACC}}q_{\text{CGT}}^2.$$

Factoring both sides gives

$$q_{\text{ACC}}q_{\text{CCA}}(q_{\text{CGT}} - q_{\text{ACC}}q_{\text{CAC}}) < q_{\text{ACC}}q_{\text{CGT}}(q_{\text{CCA}} - q_{\text{CGT}}).$$

Dividing both sides by q_{CGT} and $q_{\text{CGT}} - q_{\text{ACC}}q_{\text{CAC}}$ (which inequality (10) guarantees to be positive) implies $\frac{q_{\text{ACC}}q_{\text{CCA}}}{q_{\text{CGT}}} < \eta$. Finally, the inequality $\eta < 1$ is readily verified using inequalities (10) and (12). □ Claim

Since $\eta \in (0, 1)$, it remains only to show that $0 < a_3, a_4, a_5, a_6 < 1$ whenever $\eta < a_2 < 1$. The next two claims verify that $a_3, a_4, a_5, a_6 > 0$ whenever $\eta < a_2 < 1$.

Claim 2: If $\eta \leq a_2 < 1$ then $a_3 > 0$ and $a_5 > 0$.

Proof of Claim 2. By Eqs. (26) and (28),

$$a_3 = \frac{q_{\text{ACC}}q_{\text{CAC}} \left(a_2 - \frac{q_{\text{CGT}}}{q_{\text{CAC}}} \right)}{q_{\text{CGT}} \left(a_2 - \frac{q_{\text{ACC}}q_{\text{CCA}}}{q_{\text{CGT}}} \right)} \quad \text{and} \quad a_5 = \frac{q_{\text{CGT}} \left(a_2 - \frac{q_{\text{ACC}}q_{\text{CCA}}}{q_{\text{CGT}}} \right)}{q_{\text{CAC}}a_2 \left(a_2 - \frac{q_{\text{CGT}}}{q_{\text{CAC}}} \right)}.$$

Using the inequalities in the statement of Claim 1, it is clear by inspection of these formulas that both a_3 and a_5 are positive when $a_2 \geq \eta$. □ Claim

Claim 3: If $\eta \leq a_2 < 1$ then $a_4 > 0$ and $a_6 > 0$.

Proof of Claim 3. Assume $a_2 \geq \eta$. To show that $a_4 > 0$, we will show that both the numerator and denominator of Eq. (27) are positive. By completing the square, the denominator can be written as

$$(30) \quad q_{\text{ACC}}q_{\text{CAC}}a_2^2 - 2q_{\text{ACC}}q_{\text{CGT}}a_2 + q_{\text{ACC}}^2q_{\text{CCA}} = q_{\text{ACC}}q_{\text{CAC}} \left(a_2 - \frac{q_{\text{CGT}}}{q_{\text{CAC}}} \right)^2 + \frac{q_{\text{ACC}}}{q_{\text{CAC}}}u,$$

which is positive since $u > 0$ due to inequality (11). The numerator is also positive by (11), hence $a_4 > 0$.

Similarly, we will show $a_6 > 0$ using the same approach, namely by showing that both the numerator and denominator of Eq. (29) are positive. Positivity of the denominator follows immediately by Eq. (30). To see that the numerator is also positive, first observe that it can be written as

$$(q_{\text{CAC}}a_2 - q_{\text{CGT}})(q_{\text{CGT}}a_2 - q_{\text{ACC}}q_{\text{CCA}}) = q_{\text{CAC}}q_{\text{CGT}} \left(a_2 - \frac{q_{\text{CGT}}}{q_{\text{CAC}}} \right) \left(a_2 - \frac{q_{\text{ACC}}q_{\text{CCA}}}{q_{\text{CGT}}} \right).$$

Claim 1 implies that the right-hand side is a product of positive terms when $a_2 \geq \eta$. Hence $a_6 > 0$. □ Claim

It remains to show that $a_3, a_4, a_5, a_6 < 1$ whenever $\eta < a_2 < 1$, which we show in the next three claims.

Claim 4: If $\eta < a_2 < 1$ then $a_3 < 1$.

Proof of Claim 4. Taken together, the inequalities $\eta < a_2 < 1$ and inequality (10) imply that

$$q_{\text{ACC}}(q_{\text{CCA}} - q_{\text{CGT}}) < (q_{\text{CGT}} - q_{\text{ACC}}q_{\text{CAC}})a_2.$$

Rearranging terms gives

$$q_{\text{ACC}}q_{\text{CAC}}a_2 - q_{\text{ACC}}q_{\text{CGT}} < q_{\text{CGT}}a_2 - q_{\text{ACC}}q_{\text{CCA}}.$$

The right-hand side is positive (by Claim 1 and the assumption that $a_2 > \eta$), and hence

$$\frac{q_{\text{ACC}}q_{\text{CAC}}a_2 - q_{\text{ACC}}q_{\text{CGT}}}{q_{\text{CGT}}a_2 - q_{\text{ACC}}q_{\text{CCA}}} < 1.$$

Since the left hand side is precisely a_3 by Eq. (26), the claim follows. □ Claim

Claim 5: If $\eta \leq a_2 < 1$ then $a_4 < 1$, $a_6 < 1$, and $a_4 + a_6 < 1$.

Proof of Claim 5. By the formulas in Eq. (25) and inequality (9), $a_4 + a_6 = \frac{q_{\text{CGT}}}{q_{\text{ACC}}} < 1$. Moreover by Claim 3, $a_4, a_6 > 0$ when $a_2 \geq \eta$. Therefore $a_4 < 1$ and $a_6 < 1$. □ Claim

Claim 6: If $\eta \leq a_2 < 1$ then $a_5 < 1$.

Proof of Claim 6. Inequality (11) states that $u > 0$, so the following inequality holds for any $a_2 \in \mathbb{R}$:

$$q_{\text{CAC}} \left(a_2 - \frac{q_{\text{CGT}}}{q_{\text{CAC}}} \right)^2 + \frac{u}{q_{\text{CAC}}} > 0.$$

Expanding and rearranging terms, we can rewrite the above inequality as

$$(31) \quad q_{\text{CGT}}a_2 - q_{\text{ACC}}q_{\text{CCA}} < q_{\text{CAC}}a_2^2 - q_{\text{CGT}}a_2.$$

If $a_2 \geq \eta$, then Claim 1 implies $a_2 > q_{\text{CGT}}/q_{\text{CAC}}$, which implies that the right-hand side of Eq. (31) is positive. Therefore

$$\frac{q_{\text{CGT}}a_2 - q_{\text{ACC}}q_{\text{CCA}}}{q_{\text{CAC}}a_2^2 - q_{\text{CGT}}a_2} < 1,$$

and hence $a_5 < 1$ by Eq. (28). □ Claim

We can now finish the proof of Lemma A.4. By Claim 1, $\eta \in (0, 1)$, allowing us to choose $a_2 \in (\eta, 1)$. Letting a_3, a_4, a_5, a_6 be given by the formulas in Eq. (26)-(29), Lemma A.3 implies that $(a_2, a_3, a_4, a_5, a_6)$ is a solution to the polynomial system (25). Moreover $a_3, a_4, a_5, a_6 > 0$ (by Claims 2 and 3), and $a_3, a_4, a_5, a_6 < 1$ (by Claims 4 to 6). Hence $(a_2, a_3, a_4, a_5, a_6) \in (0, 1)^5$. Finally, $a_4 + a_6 < 1$ by Claim 5. \square

Thus, we have proven both directions of Theorem 3.1, giving a complete semialgebraic description of \mathcal{M}_1 .

APPENDIX B. THE FOURIER TRANSFORM

In this section we show how to use the Fourier transform to translate between the site pattern probabilities defined in Eq. (1) and the simplified Jukes-Cantor q -coordinates defined in Eq. (6). We also prove the uniform volume-scaling property cited in Observation 1. Accompanying code and computations for this section can be found in the supplemental materials in the file `Fourier-transform-appendix.jl`. For additional details on the Fourier transformation, see (Sturmfels and Sullivant, 2005) and (Sullivant, 2023, Chapter 15, pp. 335–370).

We begin by making the observation that a given site-pattern distribution arising from a 3-leaf network (defined in Eq. (1)) may be encoded as a point $\mathbf{p} := (p_0, p_1, p_2, p_3, p_4)^\top \in \Delta_4$, where

$$\begin{aligned} p_0 &= \Pr [X_1 = X_2 = X_3] \\ p_1 &= \Pr [X_1 \neq X_2 = X_3] \\ p_2 &= \Pr [X_1 = X_3 \neq X_2] \\ p_3 &= \Pr [X_1 = X_2 \neq X_3] \\ p_4 &= \Pr [X_1, X_2, X_3 \text{ are all distinct}]. \end{aligned}$$

Due to symmetries of the Jukes-Cantor model, there are 5 equivalence classes for the leaf-state assignment probabilities of Eq. (1), and we may take $p_{AAA}, p_{ACC}, p_{CAC}, p_{CCA}, p_{CGT}$ as our system of representatives (see The algebraic-phylogenetics collaboration (2026)). Then we observe that since $p_{AAA} = p_{CCC} = p_{GGG} = p_{TTT}$,

$$p_0 = p_{AAA} + p_{CCC} + p_{TTT} + p_{GGG} = 4p_{AAA}.$$

Similar considerations yield $p_1 = 12p_{ACC}$, $p_2 = 12p_{CAC}$, $p_3 = 12p_{CCA}$, and $p_4 = 24p_{CGT}$.

To obtain the simplified Jukes-Cantor q -coordinates, we apply the following linear change of coordinates:

$$\begin{bmatrix} q_{AAA} \\ q_{ACC} \\ q_{CAC} \\ q_{CCA} \\ q_{CGT} \end{bmatrix} = \begin{bmatrix} 1 & 1 & 1 & 1 & 1 \\ 1 & 1 & -1/3 & -1/3 & -1/3 \\ 1 & -1/3 & 1 & -1/3 & -1/3 \\ 1 & -1/3 & -1/3 & 1 & -1/3 \\ 1 & -1/3 & -1/3 & -1/3 & 1/3 \end{bmatrix} \begin{bmatrix} p_0 \\ p_1 \\ p_2 \\ p_3 \\ p_4 \end{bmatrix}.$$

The 5×5 matrix in this equation is the *specialized Fourier transformation* (The algebraic-phylogenetics collaboration, 2026), which we will denote by F . Note that $q_{AAA} = 1$ since $p_0 + p_1 + p_2 + p_3 + p_4 = 1$. Thus, to obtain the simplified Jukes-Cantor q -coordinates from a point $\mathbf{p} \in \Delta_4$, we apply the transformation $\mathcal{F} := \pi \circ F$, where π is the projection

$$\pi(x_1, x_2, x_3, x_4, x_5) = (x_2, x_3, x_4, x_5).$$

Formally, the *space of simplified Jukes-Cantor q -coordinates* is the set $\mathcal{S} := \{\mathcal{F}(\mathbf{p}) : \mathbf{p} \in \Delta_4\}$. The site pattern probabilities can be recovered from the simplified Fourier coordinates by inverting F .

The next lemma shows that \mathcal{F} scales 4-dimensional volume uniformly by the constant factor $\frac{2}{\sqrt{5}} \left(\frac{4}{3}\right)^4$.

Lemma B.1 (Volume scaling). *Let $E \subseteq \Delta_4$ be measurable. Then*

$$|\mathcal{F}(E)| = \frac{2}{\sqrt{5}} \left(\frac{4}{3}\right)^4 \cdot |E|,$$

where $|\cdot|$ denotes the 4-dimensional volume.

Proof. It is straightforward to verify that for all $\mathbf{p} = (p_0, p_1, p_2, p_3, p_4)^\top \in \Delta_4$,

$$(32) \quad \mathcal{F}(\mathbf{p}) = \mathbf{1} + A\pi(\mathbf{p})$$

where $\mathbf{1} = (1, 1, 1, 1)^\top$ and

$$A = -\frac{4}{3} \begin{bmatrix} 0 & 1 & 1 & 1 \\ 1 & 0 & 1 & 1 \\ 1 & 1 & 0 & 1 \\ 1 & 1 & 1 & 1/2 \end{bmatrix}.$$

A direct computation gives $\det(A) = -2 \left(\frac{4}{3}\right)^4$.

Further, observe that when restricted to Δ_4 , the map π is a bijection onto $\pi(\Delta_4)$, with inverse $T(u_1, \dots, u_4) = (1 - u_1 - u_2 - u_3 - u_4, u_1, u_2, u_3, u_4)^\top$. Since the 4-dimensional Jacobian of T is $\sqrt{5}$, it follows by the area formula (Krantz and Parks, 2008, Theorem 5.1.1, Chapter 5, p.125) applied to $\pi^{-1} = T$ that

$$(33) \quad |\pi(E)| = \frac{1}{\sqrt{5}} |E|.$$

for every measurable $E \subseteq \Delta_4$. Therefore, since volume is translation invariant,

$$\begin{aligned} |\mathcal{F}(E)| &= |\mathbf{1} + A\pi(E)| \\ &= |A\pi(E)| \\ &= |\det(A)| \cdot |\pi(E)| \\ &= 2 \left(\frac{4}{3}\right)^4 \cdot |\pi(E)| && \text{since } |\det(A)| = 2 \left(\frac{4}{3}\right)^4 \\ &= \frac{2}{\sqrt{5}} \left(\frac{4}{3}\right)^4 \cdot |E| && \text{by Eq. (33).} \end{aligned}$$

□

Remark 1. Lemma B.1 can be used to justify the volume claims made in Observation 1. For example, since $|\Delta_4| = \frac{\sqrt{5}}{24}$, Lemma B.1 implies that the space of simplified Fourier coordinates \mathcal{S} has 4-dimensional volume $4^3/3^5 \approx 0.263$. Since approximately 1.76% of Δ_4 is mapped to \mathcal{M}_1 (as shown in Figure 5), and since the transformation \mathcal{F} scales the 4-dimensional volume of subsets of Δ_4 uniformly, it follows that \mathcal{M}_1 occupies about 1.76% of the volume of \mathcal{S} . Hence \mathcal{M}_1 has volume $(0.0176)|\mathcal{S}| \approx 0.00464$.

Similarly, Figure 5 shows that for any $i \neq j$, approximately 0.7% of the simplex is mapped to $\mathcal{M}_i \cap \mathcal{M}_j$, and approximately 0.56% is mapped to $\mathcal{M}_1 \cap \mathcal{M}_2 \cap \mathcal{M}_3$. Therefore $|\mathcal{M}_i \cap \mathcal{M}_j| = (0.007)|\mathcal{S}| \approx 0.00184$ for $i \neq j$, and $|\mathcal{M}_1 \cap \mathcal{M}_2 \cap \mathcal{M}_3| = (0.0056)|\mathcal{S}| \approx 0.00147$.

APPENDIX C. DETAILS FOR FIGURE 9 SIMULATION

For each $\delta \in \{.01, .02, \dots, .99\}$ we simulated $n = 10^7$ random networks of the form shown in Figure 9. In particular, h_4 is the height of the network, and edges a_6 and a_4 diverge at times h_3 and h_2 respectively, and then hybridize at time h_1 . We assumed a molecular clock, so that the Fourier parameters were taken to be

$$a_i = e^{-\frac{4}{3}h_i}, \quad i = 1, 2, 3,$$

$$a_4 = e^{-\frac{4}{3}(h_2-h_1)}$$

$$a_5 = e^{-\frac{4}{3}(2h_4-h_2-h_3)}$$

$$a_6 = e^{-\frac{4}{3}(h_3-h_1)}$$

where the intervals h_1 , h_2-h_1 , h_3-h_2 , and h_4-h_3 were drawn independently and uniformly at random from the interval $(0, 0.5)$. Varying the maximum of the uniform distribution had the effect of scaling the height of the bump, with ‘proportion distinguishable’ increasing when .5 was replaced by 1 and decreasing when smaller values were used. Code for running this simulation and replicating the plot in Figure 9 can be found in the file `delta-figure-plot.jl` in the Supplementary Materials.

NEW JERSEY INSTITUTE OF TECHNOLOGY
Email address: bc479@njit.edu

UNIVERSITY OF WISCONSIN MADISON
Email address: akenglander@wisc.edu

UNIVERSITY OF HAWAI'I AT MĀNOA
Email address: joseael@hawaii.edu

UNIVERSITY OF HAWAI'I AT MĀNOA
Email address: egross@hawaii.edu

UNIVERSITY OF HAWAI'I AT MĀNOA
Email address: max6@hawaii.edu

THE COLLEGE OF WOOSTER
Email address: clong@wooster.edu

NORTH CAROLINA STATE UNIVERSITY
Email address: dolds@ncsu.edu

UNIVERSITY OF HAWAI'I AT MĀNOA
Email address: oconnor3@hawaii.edu

UNIVERSITY OF HAWAI'I AT MĀNOA
Email address: udanir@hawaii.edu

UNIVERSITY OF HAWAI'I AT MĀNOA
Email address: csum@hawaii.edu